Journal of
Materials Chemistry C

REVIEW

View Article Online
View Journal | View Issue



Cite this: J. Mater. Chem. C, 2017, 5, 5610

# Layer-controlled two-dimensional perovskites: synthesis and optoelectronics

Jakub Jagielski,† Sudhir Kumar,† Wen-Yueh Yu† and Chih-Jen Shih*

Received 2nd February 2017,
Accepted 19th May 2017

DOI: 10.1039/c7tc00538e

rsc.li/materials-c

Solution-processed hybrid organic–inorganic metal halide perovskites are emerging as one of the most promising candidates for low-cost photovoltaics and optoelectronics. Moreover, two-dimensional (2D) forms of these materials induce a dielectric quantum confinement effect that drastically increases the exciton binding energy. Previous studies on two-dimensional (2D) hybrid perovskites have been focused on the thinnest counterparts, namely, the zero-layer and monolayer species, in which the photoluminescence quantum yield is typically low (<10%), thereby limiting their applications in optoelectronics. Recent advances in colloidal synthesis have suggested that precise control over the layer numbers can be realized on a large scale, offering another degree of freedom in tailoring the optoelectronic properties. Herein, we reviewed the photophysical properties, synthetic routes, and potential technology opportunities of layer-controlled 2D hybrid perovskites.



## I. Introduction

Perovskites refer to the crystallographic structures with the general chemical formula of $ABX_3$. The first synthetic perovskite system reported in 1893 was the inorganic metal trihalide, $CsPbX_3$ (X = Cl, Br, and I).[1] The optoelectronic properties of these materials, however, were not extensively studied until the 1950s when frequency-dependent photoconductivity was demonstrated.[2] Shortly thereafter, organic–inorganic hybrid perovskites (OIHP), where the A site was an organic cation (*e.g.*, $CH_3NH_3^+$ and $CH(NH_2)_2^+$), B site was a heavy metal cation (*e.g.*, $Pb^{2+}$ and $Sn^{2+}$), and X site was a halogen anion, were further investigated.[3] The OIHP framework involves a corner-sharing network of $BX_6$ octahedral units, with the cations occupying voids within the structure.[4] The Goldschmidt's tolerance factor, $t = (r_A + r_X)/[\sqrt{2}(r_B + r_X)]$, where $r_A$, $r_B$, and $r_X$ are the ionic radii of A, B, and X, respectively, empirically predicts the stability

*Department of Chemistry and Applied Biosciences, Institute for Chemical and Bioengineering, ETH Zürich, 8093 Zürich, Switzerland.*
*E-mail: chih-jen.shih@chem.ethz.ch*
† These authors contribute equally to this work.

**Jakub Jagielski**

*Jakub Jagielski received his BSc in Chemical Engineering from ETH Zurich, Switzerland in 2014. Subsequently he worked as an intern at CSIRO, Australia, on the development of MOFs as heavy metal absorbers. In 2016 he obtained his MSc in Chemical- and Bioengineering also from ETH Zurich. In the same year he started to pursue his PhD degree in the Lab for Interface and Surface Engineering of Nano-materials led by Prof. Chih-Jen Shih at the same institution. His research activities focus on the synthesis of luminescent, 2D perovskite nanoplatelets for the fabrication of efficient and color-pure LEDs.*

**Sudhir Kumar**

*Dr. Sudhir Kumar received his PhD in Materials Science and Engineering (2014) from the National Tsing Hua University (NTHU), Taiwan. Prior to moving to ETH Zurich in 2015 he served as a postdoc at NTHU. He is now a postdoctoral fellow in the Lab for Interface and Surface Engineering of Nanomaterials at ETH Zurich, aiming at the development of energy-efficient and ultra-color pure light emitting diodes (LEDs) based on two dimensional (2D) perovskite emitters. His research interests mainly focus on the design and fabrication of organic LEDs (OLEDs), perovskite LEDs, and flexible and stretchable LEDs for next generation displays and human-friendly illumination devices.*

of an OIHP compound. Typically, the majority of these compounds form in the range of $0.8 \leq t \leq 1.0$. Other factors, such as the octahedral factor, are also used as a measure of the stability and formability of these compounds,[5] which have been well-summarized in recent review articles.[4]

Since 2009, the unprecedented success of OIHPs as low-cost semiconductor materials in next-generation photovoltaics has generated considerable research effort aimed toward understanding the underlying photophysics.[6] Indeed, unlike organic semiconductors and inorganic quantum dots (QDs), in which Frenkel-like excitons predominate,[7] recent advances in perovskite photophysics have concluded that photoexcitation generates nearly 100% free carriers in $CH_3NH_3PbI_3$ perovskites at room temperature.[8] Furthermore, the generated free carriers possess extremely long lifetime ($\sim$μs) and diffusion length ($>$μm), comparable to those in single-crystalline, defect-free semiconductors, despite the fact that a high density of defects and dynamic disorders are supposedly introduced during solution processing.[6] Several explanations have been proposed, mainly about the unique role of organic cations in OIHPs. First, the collective orientational motion of organic cations screens the electric field in the material,[9] which, in turn, results in an anomalously high dielectric constant at low frequency,[10,11] as well as a small estimated exciton binding energy, $E_B$, of 2–20 meV.[9,11–14] This facilitates long exciton lifetime. Next, the fast motion of organic cations, coupled with the transient deformation of $PbX_6$ octahedral units, could reduce carrier trapping and electron–hole recombination, possibly by creating local ferroelectric domains.[15,16] The coupled dynamics is also believed to reduce electron–hole recombination by introducing the indirect-bandgap behavior.[17–19] Very recently, new spectroscopic findings have further revealed that the formation of large polaron screens the Coulomb potential for charge carriers from charged defects.[20] Clearly, the ensemble of the above physical mechanisms delays exciton recombination in bulk OIHP systems, resulting in outstanding photovoltaic characteristics.

With proper materials engineering, in general, a good photovoltaic semiconductor also leads to good optoelectronics,[21] in which excitons are desired to radiatively recombine. However, past experience in compound semiconductors has suggested that this process often demands high materials purity and crystallinity. In this respect, the fact that the OIHP systems show higher tolerance to materials defects may imply new technology opportunities for low-cost, solution-processed optoelectronics.[6,22–24] Indeed, as compared to other large-area light emitting technologies, such as organic semiconductors[25] and inorganic QDs,[26] they have shown advantages in easy synthesis, low materials cost, and high color purity.[24] In addition, similar to inorganic QD systems, the strong spin–orbit coupling induced by heavy metal atoms in the lattice facilitates intersystem crossing,[27] so one can efficiently harvest both singlet and triplet recombinations. Recently, bright and efficient electroluminescence (EL) has been demonstrated at room temperature, based on methylammonium lead halide ($CH_3NH_3PbX_3$) and cesium lead halide ($CsPbX_3$) perovskites. To date, the most efficient devices are made by pure halides (X = Br or I), corresponding to the emission wavelength, $\lambda$, centered at $\sim$550 nm or $\sim$800 nm, respectively. For many applications such as displays, it remains challenging to attain pure red, green, and blue emitters at $\sim$650, $\sim$525, and $\sim$450 nm, respectively, with sufficiently high quantum yields (QYs).

The collective orientational motion of organic cations may have both positive and negative effects on exciton recombination, which have not yet been well addressed in literature.[8,28] On one hand, it protects excitons from recombination with charged defects, presumably reducing the Auger recombination. On the other hand, the resulting high dielectric constant and transient indirect bandgap have been proven to facilitate the formation of free carriers,[8] which makes it relatively difficult to efficiently harvest radiative recombination. In order to overcome these difficulties, one approach is to spatially confine the diffusion of carriers, thereby increasing the probability for them to meet

**Wen-Yueh Yu**

*Dr. Wen-Yueh Yu obtained his PhD in Chemical Engineering under the supervision of Professor C. Buddie Mullins at the University of Texas at Austin. He is currently a postdoctoral researcher in Professor Chih-Jen Shih's group at the Institute for Chemical and Bioengineering, ETH Zurich, where his research focuses on the synthesis and photophysics of two-dimensional hybrid organic–inorganic perovskites. His research interests lie in nanotechnology, surface science and catalyst chemistry with a particular interest in their application in sustainable energy technologies and green chemistry processes.*

**Chih-Jen Shih**

*Professor Chih-Jen Shih received his PhD degree in Chemical Engineering from Massachusetts Institute of Technology in 2014, under the supervision of Professors Daniel Blankschtein and Michael Strano. Then he served as a postdoctoral researcher in Zhenan Bao's group at Stanford University. He is currently a tenure-track assistant professor of chemical engineering at the Department of Chemistry and Applied Biosciences, ETH Zurich. His research interest lies in understanding and engineering the interfaces formed between 2D and 3D materials, for the applications of functional surfaces and optoelectronics.*

each other. For example, by reducing the perovskite grain size down to ~100 nm in the bulk OIHP systems,[29] the exciton diffusion length significantly reduces;[30] therefore, high external quantum efficiency (EQE) in the light emitting diode (LED) device has been demonstrated.[29] Nevertheless, this method does not allow the facile manipulation of $\lambda$ with mixed halides.[31] Recent findings also suggested that the photoluminescence (PL) QY, which essentially represents the upper limit of the internal quantum efficiency (IQE) in an LED device,[26] tends to decrease upon mixing halides. In addition, fabricating an ultrathin perovskite film with complete substrate coverage has been proven to be technically difficult.[24]

Following the path of compound semiconductors, a straightforward approach is to make the material more excitonic[8] by the effect of reduced dimensionality,[32,33] namely, the quantum confinement effect, so that one can tune the bandgap width by the particle size. An interesting feature of the OIHP systems is that the excitonic Bohr radius, $a_B$*, is estimated to be only ~1.4–2.0 nm,[34,35] comparable to the lattice constant of the OIHP unit cell (~0.6 nm). Consequently, the bandgap change appears only for relatively small particles and is expected to be quantized with their size. Two-dimensional (2D) perovskites, which can be described by $A'_2[ABX_3]_nBX_4$, where A′ is a long-chain ligand cation and $n$ is the stacking number of perovskite unit cells,[36] are found to be the most stable forms of quantum-confined perovskites.[3] As stated before, a consequence of reduced dimensionality is the enhancement of the exciton binding energy. In an ideal 2D quantum well, nevertheless, the binding energy increase does not exceed four times, as predicted by the quantum mechanical calculations.[37] In order to further enhance the binding energy, another strategy, namely, the dielectric quantum confinement effect (which takes advantage of the low dielectric constant of the organic ligands), has been utilized to induce stronger Coulombic interactions between electrons and holes.[38] Theoretically, it has been suggested that an increase of exciton binding energy up to 100 times can be achieved in thin wells.[39] However, in practice, this enhancement is observed to be about one order of magnitude lower than the theoretical prediction.[40] Furthermore, the long-range nature allows the extension of this effect to thick wells ($>5\ a_B$*).[39]

With the above fundamental background in mind, we believe the quantum-confined, layer-controlled 2D hybrid perovskites would be a promising candidate toward next-generation large-area optoelectronics. In this account, we review the synthesis and potential optoelectronic applications of 2D hybrid perovskites, complementary to several recent reviews,[3,4,41–43] which are more focused on the structural and physical properties of 2D perovskites. Note that in this article, the defined $n$ for $A'_2[ABX_3]_nBX_4$ is one layer lower than convention,[3] in order to stress the importance of the organic cations A, and therefore, $n$ = 0 represents the thinnest 2D perovskite, $A'_2BX_4$.

## II. Non-colloidal synthesis

We first review the synthesis of thin perovskite platelets with the $CH_3NH_3PbX_3$ (X = Cl, Br, and I) structure. Note that these perovskites are essentially non-layered materials that lack a van der Waals (vdW) gap between the layers in their 3D structural framework.[44] The non-layered feature makes it relatively difficult for the top-down synthesis of thin $CH_3NH_3PbX_3$ perovskites from their bulk material by mechanical exfoliation, the typical strategy to obtain thin layers from 2D layered materials.[45] In the first part of this section, a number of non-colloidal methods based on vapor-phase-based approaches[44,46–49] for bottom-up synthesis of thin $CH_3NH_3PbX_3$ perovskite platelets are briefly summarized as follows. We note that only the latest study[48] that combines the solution process and vapor-phase conversion successfully yielded $CH_3NH_3PbX_3$ perovskite platelets in a 2D form (with a thickness as thin as a single unit cell); other studies[44,46,47,49] are included in order to provide a complete account for the development history of these vapor-phase-based methods.

Xiong and co-workers synthesized $CH_3NH_3PbX_3$ perovskite nanoplatelets (NPLs) (presumably $n > 10$, where $n$ represents the number of layers) using a two-step vapor-phase process.[44] It involved (i) the vdW epitaxy of lead halide NPLs and (ii) the gas-solid heterogeneous reaction with methylammonium halide vapor, as shown in Fig. 1a. The first step was performed by placing lead halide powders upstream that were heated under low vacuum in a continuous hydrogen/argon gas flow. The lead halide platelets can be, therefore, formed downstream on a muscovite mica substrate. The lead halide platelets prepared in step (i) were then converted to perovskites by a reaction with evaporated methylammonium halide. The prepared $CH_3NH_3PbX_3$ perovskite NPLs typically show a lateral size of 5 to 30 μm, with a thickness from tens to hundreds of nanometers (see Fig. 1b).[44] The same method was used to synthesize the mixed halide perovskite platelets by intercalating gaseous $CH_3NH_3Cl$ and $CH_3NH_3Br$ molecules into the $PbI_2$ platelets. The synthesis strategy forms the basis of non-colloidal synthesis of thin perovskites platelets. Following a similar approach, Niu *et al.* have synthesized $CH_3NH_3PbI_3$ perovskite platelets on a number of inorganic 2D materials, including graphene, hexagonal boron nitride (h-BN), and molybdenum disulfide ($MoS_2$).[46] It seems the 2D nature of these materials facilitates the vdW epitaxy of layered $PbI_2$. Preferential growth of thin perovskites platelets on patterned h-BN islands was demonstrated.[46]

Wang *et al.* developed a one-step vdW epitaxy method[47] to grow thin $CH_3NH_3PbCl_3$ perovskite platelets on the muscovite mica substrate directly from organic and inorganic precursors (Fig. 1c). They simultaneously placed all the precursors and the substrate in an alumina tube followed by heating under low vacuum with argon as the carrier gas. The positions for both the precursors and the substrate in the system were carefully designed to control the deposition and reaction temperatures. Specifically, $PbCl_2$ powder was placed in the center of the furnace at ~360 °C, and $CH_3NH_3Cl$ powders and muscovite mica substrate were placed in the upstream and downstream regions of the furnace, respectively, at ~200 °C. The perovskite platelets prepared by this one-step method are square-shaped with sub-10 nm thickness and a few tens of micrometers in lateral dimensions (Fig. 1d).[47] Note that the thin perovskite platelets fabricated by the vapor-phase-based methods tend to

 

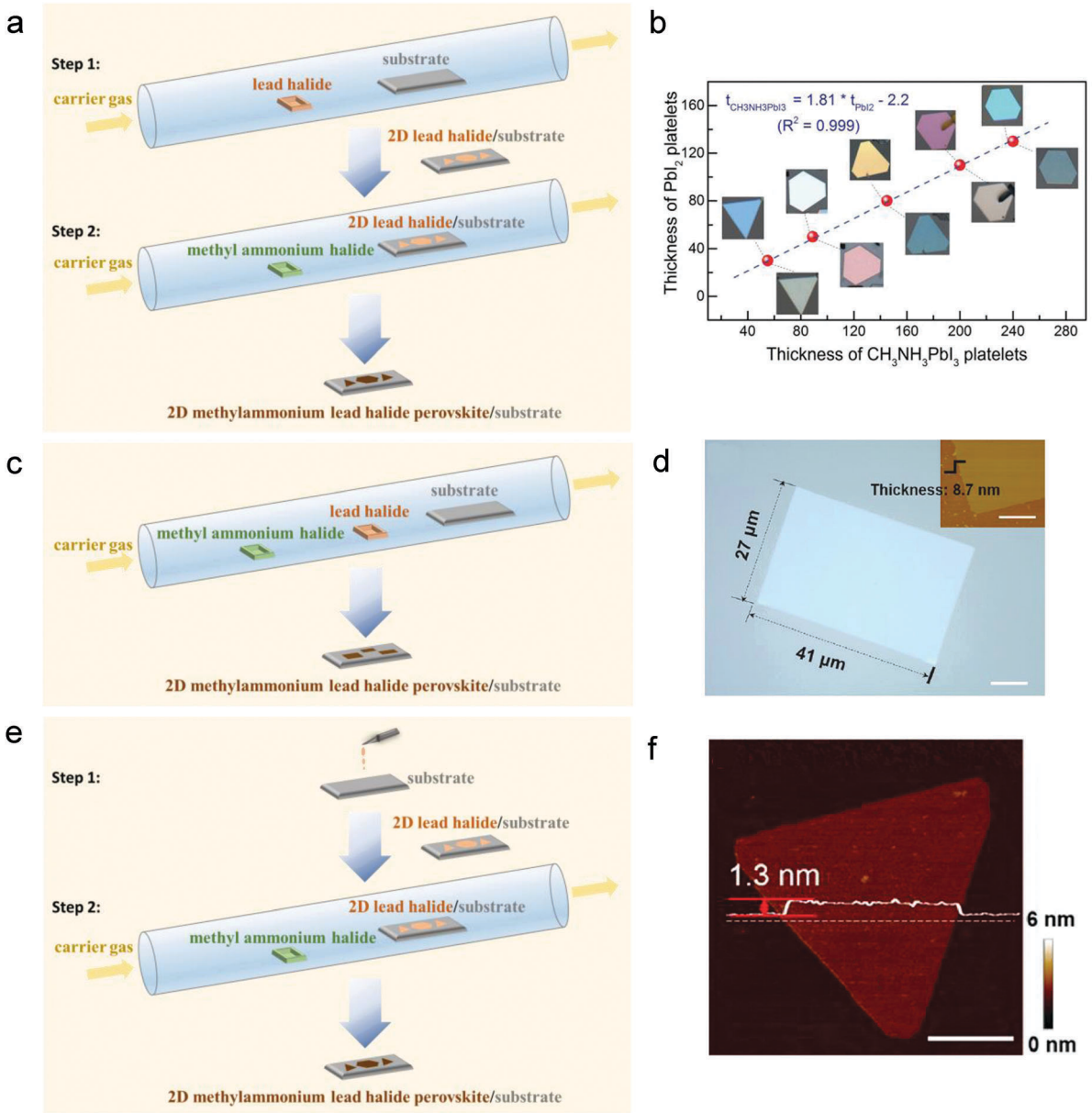


Fig. 1 (a) Schematic illustration of two-step vapor-phase process, and (b) the measured thicknesses and optical images of initial $PbI_2$ nanoplatelets and corresponding $CH_3NH_3PbI_3$ platelets. Reproduced with permission. Copyright 2014, Wiley-VCH.[44] (c) Schematic illustration of one-step VDW epitaxy method, and (d) the optical and AFM images (scale bars = 10 μm) of a $CH_3NH_3PbI_3$ nanosheet. Reproduced with permission. Copyright 2015, American Chemical Society.[47] (e) Schematic illustration of combined solution process and vapor-phase conversion method, and (f) the AFM image (scale bar = 2 μm) of a $CH_3NH_3PbI_3$ nanosheet. Reproduced with permission. Copyright 2016, American Chemical Society.[48]

be relatively thick (typically, $n > 20$). By combining observations of the fractal evolution of perovskite platelets and the Monte Carlo calculations, it was proposed[47] that the absence of mono- and few-layer 2D perovskites from the one-step vdW epitaxy method results from a high vdW-type diffusivity (both surface and edge diffusivities) and low cohesive energy of perovskites. It was suggested[47] that the further treatment of substrates, such as surface passivation, might facilitate the growth of thin-layer 2D perovskites.

Very recently, Liu *et al.* successfully synthesized thin 2D $CH_3NH_3PbI_3$ perovskites by combining the solution process and vapor-phase conversion[48] (Fig. 1e), which can be viewed as an improved version of the two-step vapor-phase process.[44] In the first step, the $PbI_2$ NPLs were prepared by drop-casting the saturated $PbI_2$ aqueous solution onto a $SiO_2$/Si substrate at mild temperatures (30–180 °C). The synthesized $PbI_2$ platelets were then converted into $CH_3NH_3PbI_3$ platelets by the gaseous phase reaction at low vacuum. The synthesized $CH_3NH_3PbI_3$ platelets are triangular or hexagonal, following the morphological features of the parent $PbI_2$ ones. The thickness can be significantly reduced down to 1.3 nm (Fig. 1f),[48] while the degree of blue shift in the PL spectra is not as significant as expected.

A similar approach was also employed in another study,[49] in which the wafer-scale growth of $CH_3NH_3PbI_3$ perovskite microplate arrays was reported. Prior to growing $PbI_2$ microplate arrays, the $SiO_2$/Si substrate was patterned with hydrophobic octadecyltrichlorosilane (OTS) using photolithography. An array of $PbI_2$ seeds was selectively formed by flowing $PbI_2$ aqueous solution over the surface. The seeded substrate was then immersed into a saturated $PbI_2$ aqueous solution for growing $PbI_2$ platelets, followed by exposure to $CH_3NH_3I$ vapor to form perovskite platelets.

The vapor-phase-based methods are summarized in Table 1. To date, these methods do not allow the preparation of layer-controlled 2D perovskites on a large scale, thereby limiting their applications in optoelectronics. In addition, only a small degree of blue shift in the PL spectra had been introduced using these methods. The underlying mechanisms are still not well understood.

Next, we review the synthesis of 2D perovskites with $A'_2[ABX_3]_nBX_4$ structures, namely, the Ruddlesden–Popper perovskites. Structurally derived from the bulk $ABX_3$ analogue, three subgroups of layered perovskites are as follows: $A'_2[ABX_3]_nBX_4$ ($\langle 100\rangle$-oriented), $A'_2[ABX_3]_mX_2$ ($\langle 110\rangle$-oriented), and $A'_2[ABX_3]_qBX_6$ ($\langle 111\rangle$-oriented).[4] Among these structures, the $A'_2[ABX_3]_nBX_4$ structure has the richest family members,[4] and it is referred to as 2D perovskites in this review, as schematically shown in Fig. 2a. Clearly, $n = \infty$ and $n = 0$ represent the bulk and thinnest forms of perovskite materials, respectively. To derive from the bulk non-layered structure to the layer-controlled 2D counterpart, the A cations on the surface are often replaced by bulky, long-chained cations A′, confining the $ABX_3$ layers in a 2D manner.[50] In the 2D perovskites, $A'_2[ABX_3]_nBX_4$, $RNH_3^+$ is the most representative A′ cation ligand group, acting as a spacer between the perovskite layers.[51] Recently, the synthesis of single-crystalline 2D $(RNH_3)_2[CH_3NH_3PbX_3]_nPbX_4$ perovskites has been reported using a number of methods including silica-gel,[38,52] solvent-evaporation,[38,53] mixed-solvent-evaporation,[54–59] and liquid-phase crystallization.[50,51,56,60–64] We highlight the main findings below.

Ishihara *et al.* synthesized a series of zero-layered perovskite crystals ($n = 0$) with different alkyl group lengths and studied their optical properties,[38] *i.e.*, $(C_xH_{2x+1}NH_3)_2PbI_4$ ($x$ = 8, 9, 10, and 12) using the silica-gel method.[38] Specifically, $Pb(CH_3COO)_2$, $C_xH_{2x+1}NH_2$, $CH_3COOH$, and $Na_2SiO_3$ were mixed in water and gelled. After about one week, KI aqueous solution was then added onto the gel to introduce iodide ions. Square crystals with a typical size of $2 \times 2 \times 0.1$ mm$^3$ were gradually formed after one month. The silica-gel method was found to be ineffective for shorter ligands ($x$ = 4 and 6), and therefore, these crystals were prepared simply by slowly evaporating the aqueous precursor solution that contains a stoichiometric amount of $C_xH_{2x+1}NH_3I$ and $PbI_2$,[38] yielding small crystals of $\sim 1 \times 1 \times 0.03$ mm$^3$. It was found that the crystals prepared by the silica-gel method[38,52] are easily contaminated by the gel residues and the hardness of the gel was rather difficult to control.[56] A cleaner method using mixed acetone/nitromethane solution was subsequently reported by the same group using the R group with $x = 10$.[54–56] The resulting $(C_{10}H_{21}NH_3)_2PbI_4$ crystals are relatively large, up to $4 \times 10 \times 0.1$ mm$^3$.[56] The bromide counterpart, *i.e.*, $(C_{10}H_{21}NH_3)_2PbBr_4$ crystals, with a typical size of $3 \times 3 \times 0.05$ mm$^3$ were also prepared by the same method, but using water to replace acetone due to the low solubility of $(C_{10}H_{21}NH_3)_2PbBr_4$ in acetone. They also reported the synthesis of $(C_{10}H_{21}NH_3)_2PbCl_4$ crystals. Another commonly used ligand group, phenethylammonium, *i.e.*, $C_6H_5C_2H_4NH_3$, is also adopted.[59] Mitzi also reported the synthesis of $C_4H_9NH_3PbI_4$ ($n = 0$) perovskites using a liquid-phase crystallization method.[60] The same method was also employed to prepare 2D perovskites with larger $n$ ($n$ = 1 and 2).[61,62] Kanatzidis and co-workers synthesized $(C_4H_9NH_3)_2[CH_3NH_3PbX_3]_nPbI_4$ crystals with $n$ = 0, 1, 2, and 3 (Fig. 2b) in a hot aqueous solution containing HI, $H_3PO_2$, and PbO, followed by adding $C_4H_9NH_2$ to the solution during the cooling process.[50,51] The amount of $C_4H_9NH_2$ determines $n$.[51] Table 2 briefly summarizes the samples and methods described above.

Table 1 Summary of the main vapor-phase-based methods for synthesizing thin organic–inorganic hybrid perovskites with the $CH_3NH_3PbX_3$ (X = Cl, Br, and I) structure

| Perovskite material | Synthesis method |
|---|---|
| Pure halide | |
| $CH_3NH_3PbCl_3$ | Two-step vapor-phase process[44] |
| $CH_3NH_3PbCl_3$ | One-step vdW epitaxy method[47] |
| $CH_3NH_3PbBr_3$ | Two-step vapor-phase process[44] |
| $CH_3NH_3PbBr_3$ | Combined solution process and vapor-phase conversion[48] |
| $CH_3NH_3PbI_3$ | Two-step vapor-phase process[44] |
| $CH_3NH_3PbI_3$ | Combined solution process and vapor-phase conversion[48] |
| Mixed halide | |
| $CH_3NH_3PbCl_xI_{3-x}$ | Two-step vapor-phase process[44] |
| $CH_3NH_3PbBr_xI_{3-x}$ | Two-step vapor-phase process[44] |
| $CH_3NH_3PbBr_xI_{3-x}$ | Combined solution process and vapor-phase conversion[48] |

The synthesized single crystals, nevertheless, do not allow solution processing for large-area, thin-film optoelectronics. Recently, synthetic concepts were adopted to achieve direct solution-phase growth of 2D $(RNH_3)_2PbX_4$ perovskite single crystals.[64,65] Specifically, Gauthron *et al.* prepared $(C_6H_5C_2H_4NH_3)_2PbI_4$ ($n = 0$) thin films by spin-coating the precursor/dimethylformamide (DMF) solution on a quartz substrate.[65] Self-organization occurred during the spin-coating process, resulting in the formation of $(C_6H_5C_2H_4NH_3)_2PbI_4$ perovskite crystals. Film thickness ranging from 3 to 100 nm can be obtained by controlling the concentration of the precursor solution. Yang and colleagues also reported the direct solution-phase growth of thin 2D $(C_4H_9NH_3)_2PbBr_4$ perovskite ($n = 0$) platelets (Fig. 2c) using the ternary co-solvent system.[64] This method was also applied to prepare mixed-halide 2D perovskites, such as $(C_4H_9NH_3)_2PbCl_2Br_2$, and $(C_4H_9NH_3)_2PbBr_2I_2$, but all with $n = 0$.

The methods discussed above[64,65] mostly yield $A'_2BX_4$ 2D perovskites (*i.e.*, $n = 0$) and lack good control on $n$ (particularly for $n > 3$). Furthermore, most of these methods produce small crystals in solution, which are not suitable for large-area optoelectronics that essentially require (i) thickness control down to 10–100 nm and (ii) complete surface coverage. For

 

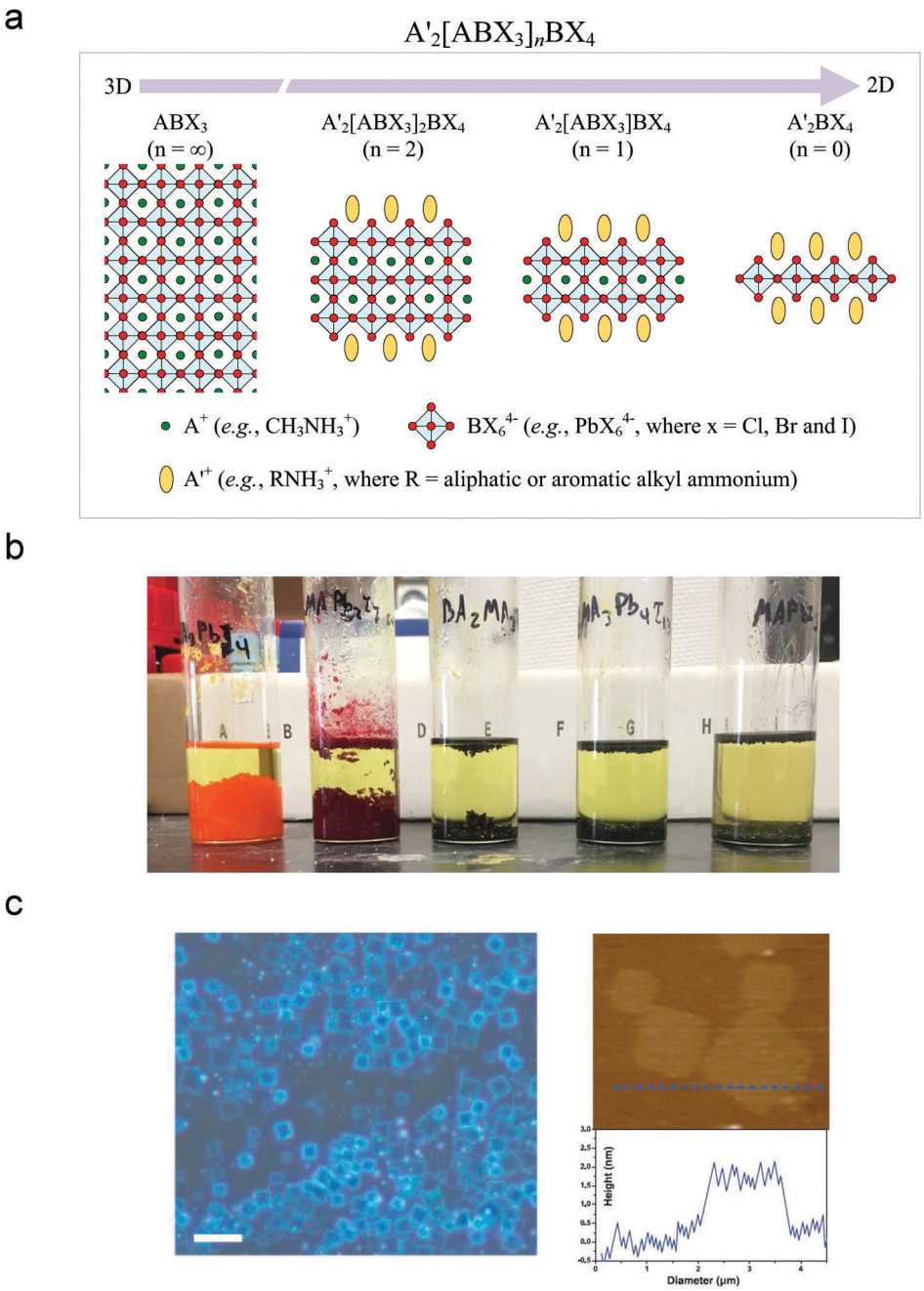


Fig. 2 (a) Schematic structures of 2D $A'_2[ABX_3]_nBX_4$ perovskites ($n$ = 0, 1 and 2) and the 3D $ABX_3$ perovskite ($n$ = ∞). (b) SEM images (top; scale bars = 200 μm) and photographs (bottom) of $(C_4H_9NH_3)_2[CH_3NH_3PbX_3]_nPbI_4$ perovskite crystals ($n$ = 0, 1, 2, 3 and ∞). Reproduced with permission. Copyright 2016, American Chemical Society.[51] (c) Optical image (top; scale bar = 10 mm) and AFM image of the 2D $(C_4H_9NH_3)_2PbBr_4$ perovskite ($n$ = 0) crystals. Reproduced with permission. Copyright 2015, the American Association for the Advancement of Science.[64]

optoelectronic applications, it remains challenging to simultaneously engineer solution chemistry and self-assembly process.

## III. Colloidal synthesis

Motivated by the necessity of solution-processed optoelectronic devices that require ease and low cost of fabrication, 2D perovskites in the form of colloidal nanocrystals (NCs) emerged as a potential alternative to inorganic colloidal QDs.[26] Following the concepts developed during that time, a variety of methods have been proposed to synthesize colloidal dispersions based on perovskite compounds. The first successful synthesis of $CH_3NH_3PbBr_3$ nanoparticles was reported in 2014 by Schmidt *et al.* by mixing $CH_3NH_3Br$ and long-chain alkyl ammonium bromide with $PbBr_2$ dissolved in DMF with octadecene containing oleic acid at room temperature.[66] The formation of NCs was triggered by the low solubility of perovskite precursors in a nonpolar solvent, with the

Table 2 Selected literature for the synthesis methods of 2D organic–inorganic hybrid perovskites with the $(RNH_3)_2(CH_3NH_3PbX_3)_nPbX_4$ (X = Cl, Br, and I) structure

| Perovskite material | Synthesis method[a] |
|---|---|
| **n = 0** | |
| *R = aliphatic alkyl group* | |
| $(C_4H_9NH_3)_2PbBr_4$ | LPC[64] |
| $(C_4H_9NH_3)_2PbI_4$ | LPC[50,51,60–62] |
| $(C_6H_{13}NH_3)_2PbI_4$ | SE(acetone)[53] |
| $(C_{10}H_{21}NH_3)_2PbCl_4$ | LPC[56] |
| $(C_{10}H_{21}NH_3)_2PbBr_4$ | MSE($H_2O$/NM)[56] |
| $(C_{10}H_{21}NH_3)_2PbI_4$ | SG,[52] MSE(acetone/NM)[56] |
| $(C_xH_{2x+1}NH_3)_2PbBr_4$ ($x$ = 2, 3, 4, 6 and 10) | MSE(DMF/acetone)[58] |
| $(C_xH_{2x+1}NH_3)_2PbI_4$ ($x$ = 4 and 6) | SE($H_2O$)[38] |
| $(C_xH_{2x+1}NH_3)_2PbI_4$ ($x$ = 8, 9, 10 and 12) | SG[38] |
| *R = aromatic alkyl group* | |
| $(C_6H_5C_2H_4NH_3)_2PbI_4$ | MSE(acetone/NM,[54–56] THF/ether[57]) |
| **n = 1** | |
| *R = aliphatic alkyl group* | |
| $(C_4H_9NH_3)_2(CH_3NH_3PbI_3)PbI_4$ | LPC[50,51,60–62] |
| $(C_6H_{13}NH_3)_2(CH_3NH_3PbI_3)PbI_4$ | SE(DMF)[53] |
| $(C_xH_{2x+1}NH_3)_2(CH_3NH_3PbBr_3)PbBr_4$ ($x$ = 2, 3, 4 and 6) | MSE(DMF/acetone)[58] |
| *R = aromatic alkyl group* | |
| $(C_6H_5C_2H_4NH_3)_2(CH_3NH_3PbI_3)PbI_4$ | MSE(acetone/NM,[54–56] THF/ether[57]) |
| **n = 2** | |
| *R = aliphatic alkyl group* | |
| $(C_4H_9NH_3)_2(CH_3NH_3PbI_3)_2PbI_4$ | LPC[50,51,60–63] |
| $(C_6H_{13}NH_3)_2(CH_3NH_3PbBr_3)_2PbBr_4$ | MSE(DMF/acetone)[58] |
| $(C_6H_{13}NH_3)_2(CH_3NH_3PbI_3)_2PbI_4$ | SE(DMF)[53] |
| *R = aromatic alkyl group* | |
| $(C_6H_5C_2H_4NH_3)_2(CH_3NH_3PbI_3)_2PbI_4$ | MSE(acetone/NM)[59] |
| **n = 3** | |
| *R = aliphatic alkyl group* | |
| $(C_4H_9NH_3)_2(CH_3NH_3PbI_3)_3PbI_4$ | LPC[50,51,63] |

[a] DMF: dimethylformamide; LPC: liquid-phase crystallization; MSE: mixed-solvent-evaporation; NM: nitromethane; SE: solvent-evaporation; SG: silica-gel: THF: tetrahydrofuran.

alkyl ammonium ions acting as capping ligands that limit the growth of NCs. It results in highly luminescent and stable dispersions with the peak emission at ~525 nm (Fig. 3a). Further optimization of perovskite precursors and ligand concentrations enable a high value of PLQY ~83% (Fig. 3b) in solution.[67] Note that even in the inorganic QD systems, it often requires the core–shell structure to attain this value. Subsequently, Protesescu and co-workers synthesized $CsPbX_3$ nanocubes based on the hot-injection method—a tool formerly used to prepare QDs.[33] In this work, the effects of halide composition on the bandgap width and the optical properties were demonstrated (Fig. 3c). Although the $CsPbX_3$ perovskites are known to crystallize in orthorhombic, tetragonal, or cubic structures,[4] at a high temperature, only the cubic phase is formed in all the compounds. At room temperature, particularly for $CsPbI_3$ NCs, the cubic phase has proven to be metastable.[4] Nevertheless, after cooling down to room temperature, all the compositions of $CsPbX_3$ NCs are with the cubic phase, suggesting that the reduction of crystal size might stabilize this particular phase.

Note that the synthesized perovskite NCs only exhibit a very small degree of PL blue shift compared to that in the bulk. This reflects the fact that the Bohr radius in the perovskite systems is small, and the size of NCs is not sufficiently small to reach the quantum-confinement level. Nevertheless, the PLQYs in these compounds are still amazingly high, compared to that in large single crystals (typically with PLQY <1%).[68] This implies, unlike in inorganic QD systems, that quantum confinement does not seem to be a prerequisite to reach high PLQY. However, as we mentioned in Section I, the transformation of mixed-halide perovskite NCs by means of the halide-exchange reaction has been proven to significantly reduce their PLQY,[68] thereby preventing them from being used in advanced applications in optoelectronics. This motivates researchers to synthesize colloidal, layer-controlled 2D perovskites.

The first observation of colloidal, quantum-confined 2D perovskites is reported by Tyagi *et al.* in early 2015.[36] A slight modification of the colloidal synthesis method results in the formation of mixed perovskite nanostructures with different morphologies, and by purifying this mixture of colloidal dispersions by dilution, filtration, precipitation, and re-dispersion, the 2D NPLs of $CH_3NH_3PbBr_3$ with different thicknesses were isolated. Although the PL spectrum showed a predominant peak at ~530 nm, which is associated with the bulk phase, a sharp excitonic feature at 431 nm, or a ~0.5 eV blue-shift compared to the bulk, appeared in its absorption spectrum. By comparing with previous experimental work based on non-colloidal synthesis, this peak was identified to correspond to 2D $CH_3NH_3PbBr_3$ perovskite with $n$ = 1 (see Fig. 4a). The minor components in the PL spectrum centered at 475, 490, and 504 nm were also found to correspond to $n$ = 4, 5, and 6, respectively. The lateral size of the synthesized NPLs was up to hundreds of nanometers.

A synthesis method toward control over $n$ was later proposed to tune $\lambda$ (Fig. 4b).[69] The idea encompasses the use of both long octylammonium (OA) and short methylammonium (MA) cations together with $PbBr_2$ dissolved in DMF and introduced to toluene. The former cannot be incorporated into the perovskite crystal structure and instead binds with the alkyl chain sticking outward, thus arresting crystal growth in the dimension along the hydrocarbon chain. By increasing the ratio of OA to MA, the thickness of the produced NPLs is, therefore, reduced. The PL emission changed gradually from green (0% OA), blue-green (70% OA), blue (90% OA), and finally to violet (100% OA). Nevertheless, except for the green ($n = \infty$) and violet dispersions ($n$ = 0), the emission spectra exhibited multiple peak components, suggesting that the resulting dispersions are not sufficiently pure. In addition, the reported PLQYs are typically <10%. Apart from change of the PL emission, in this report,[69] another important observation is that along with the rectangular NPLs, the transmission electron microscopy (TEM) images revealed quasi-spherical objects, roughly 6 nm in diameter, which were proven to be a degradation product of the perovskite nanostructures. It has made atomic-level electron microscopic imaging of colloidal 2D hybrid perovskites very challenging.

 

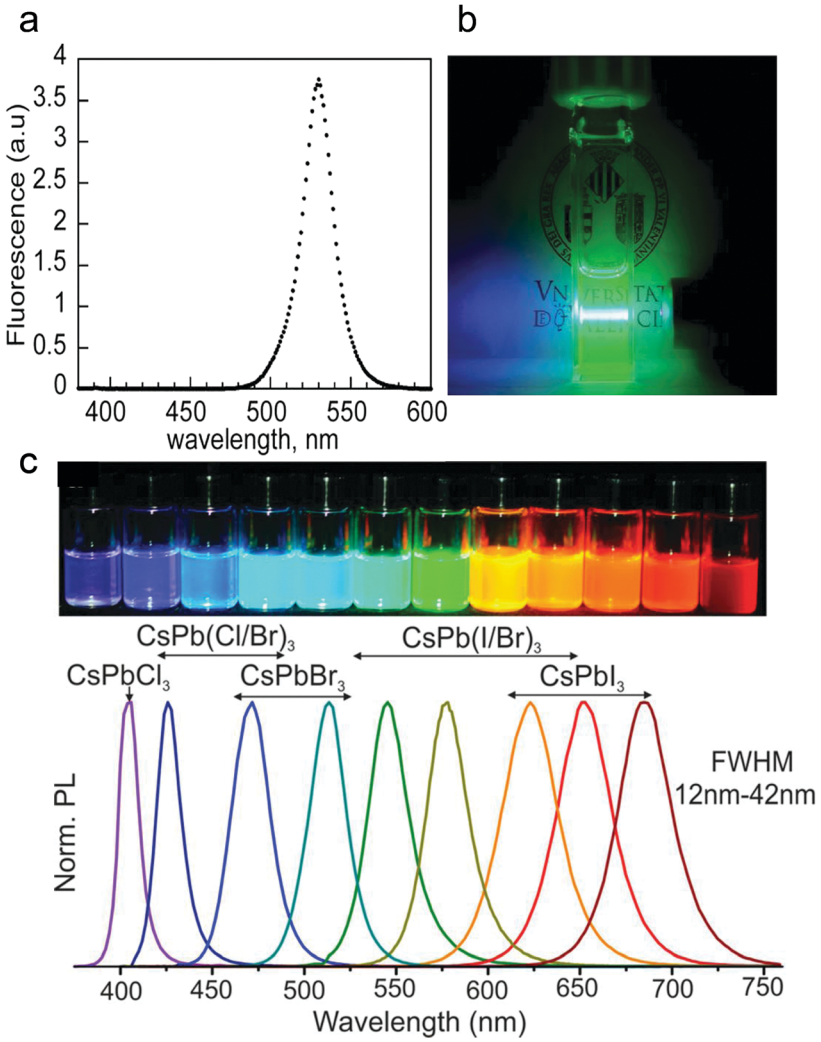


Fig. 3 (a) Room temperature fluorescence spectra of $MAPbBr_3$ nanocrystals[66] and (b) a photograph of the colloidal dispersion containing $MAPbBr_3$ nanocrystals under UV-light.[67] Reproduced with permission. (a) Copyright 2014, American Chemical Society,[66] (b) Copyright 2015, Royal Society of Chemistry.[67] (c) Colloidal solutions of $CsPbX_3$ nanocubes under UV lamp together with the respective PL spectra. Reproduced with permission. Copyright 2015, American Chemical Society.[33]

Vybornyi and co-workers also reported another synthesis method of $CH_3NH_3PbX_3$,[70] which does not involve DMF or other polar solvents. The reaction between methylamine ($CH_3NH_2$) and $PbX_2$ is conducted in a high-boiling nonpolar solvent (*e.g.*, 1-octadecene, ODE) at elevated temperatures in the presence of oleylamine (OLM) and oleic acid (OLA) as coordinating ligands. The $PbX_2$ salt serves as both the $Pb^{2+}$ and $X^-$ source, and the proton is provided by OLA to form $CH_3NH_3^+$. The tetrahydrofuran (THF) solution containing methylamine and OLA is injected into $PbX_2$ solubilized in the ODE/OLM/OLA mixture under vigorous stirring, resulting in the formation of NCs within seconds. By adjusting the amount of OLM, the method selectively yields either blue-emitting square NPL-like NCs or green-luminescent nanowires. The platelets exhibited an absorption peak at ~450 nm and a single PL emission peak at 465 nm with PLQY of 18% (Fig. 4c), approximately corresponding to $n = 3$.[58] On the other hand, a lower content of OLM promoted the aggregation of nanoparticles and formed wire-like structures, exhibiting a PL peak centered at 532 nm and a sharp absorption band with moderate excitonic component at around 520 nm. This method was also used to prepare $MAPbI_3$ NC and NPL colloidal solutions, which exhibit PL emission at ~750 and ~700 nm, respectively.

Bekenstein *et al.* reported the colloidal synthesis of CsPbX3 NPLs[71] by modifying the protocol that produces $CsPbX_3$ NCs at 140–200 °C.[33,72] They found that synthesis at a lower temperature (90–130 °C) favors 2D perovskite formation. The reaction was carried out in a flask in which $PbBr_2$ was solubilized by mixing with ODE containing OLM and OLA that acted as ligands at a later stage. Due to the low solubility of CsBr in DMF, it was necessary to degas $Cs_2CO_3$ in the presence of OLA in order to transform it into liquid Cs-oleate, as pioneered by Protesescu *et al.*[33] The reactions conducted at 130 °C produced NPL dispersions with cyan emission (corresponding to $n \sim 5$). Further decrease of the reaction temperatures to 90–100 °C induced the formation of very thin NPLs. This trend followed; nevertheless, the reaction at 70 °C did not take place, presumably

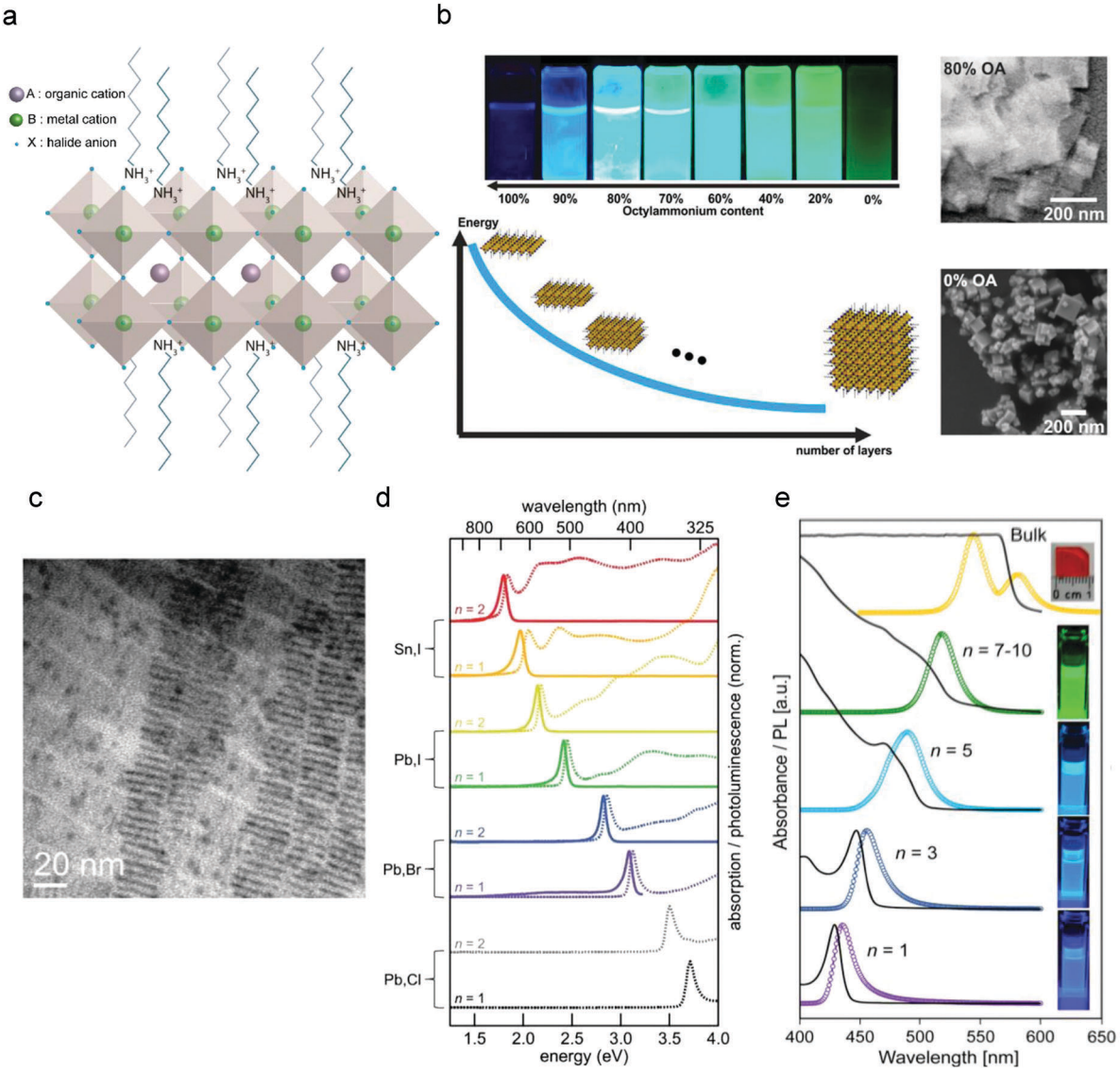


Fig. 4 (a) Images of $MAPbBr_3$ colloidal suspensions with different OA content excited with UV light together with a schematic describing quantum confinement effects in perovskite nanocrystals. The right panel shows TEM images of these nanostructures. Reproduced with permission. Copyright 2015, American Chemical Society.[69] (b) Schematic illustration of 2D perovskite nanoplatelet with $n$ = 1. Reproduced with permission. Copyright 2015, American Chemical Society.[36] Below the dependence of PL and absorption spectra of (c) 2D $MAPbBr_3$ on different layer number[68] and (d) 2D perovskites on variable chemical composition.[74] Reproduced with permission. (c) Copyright 2016, American Chemical Society,[68] (d) Copyright 2016, American Chemical Society.[74] (e) TEM image of stacked 2D $MAPbBr_3$ nanoplatelets with $n$ = 3. Reproduced with permission. Copyright 2016, Royal Society of Chemistry.[70]

because of the low reactivity of Cs-oleate at low temperatures. Although the manipulation of the reaction conditions causes certain variations, the resulting solutions are still polydispersed, containing NPLs with different thicknesses. The PL emission maxima were identified at 488, 477, 462, 435, and 405 nm, where they may be roughly assigned to NPLs with $n$ = 5, 4, 3, 1, and 0, respectively. PLQYs of 84, 45, and 10% were achieved for samples with $n$ = 5, 4, and 3, respectively (need to check). A procedure that yields monodispersed $CsPbBr_3$ NPLs was developed by Akkerman *et al.*[73] Cs-oleate, $PbBr_2$, OLM, and OLA were mixed in ODE at room temperature, followed by adding different amounts of HBr that protonates the long-chain amine. A significant amount of acetone was added at the end to initiate the nucleation of NPLs. Depending on the amount of HBr, they reported monodispersed $CsPbBr_3$ NPL dispersions that emit at 438, 449, and 459 nm corresponding to $n$ = 3, 4, and 5, respectively. The PLQY for the $n$ = 5 solution reaches 31%.

Very recently, the demand for covering possibly the largest range of the visible spectrum was addressed by Weidman and co-workers.[74] A high degree of spectral tunability was achieved through the variation of cation (A), metal (B), and halide (X) composition, as well as $n$, (Fig. 4d) in colloidal synthesis. The thin NPL dispersions of $A'_2[ABX_3]_nBX_4$ were synthesized by a nonsolvent crystallization method. Precursor salts (AX, $BX_2$, and A′X) were

 

dissolved in DMF, mixed in proper proportions, and injected into nonpolar toluene phase to obtain either $n$ = 0 or $n$ = 1 NPL solutions. Small-angle X-ray diffraction patterns were used to characterize NPL stacking. However, they observed poor colloidal stability for thick NPLs ($n > 1$) and low PLQYs (up to 22%) for thin NPLs. These issues were recently addressed by our group, in which we reported a new colloidal synthesis method that produces the quantum-confined, colloidal 2D perovskites with precisely controlled odd layer number from $n$ = 7–10 to $n$ = 1.[68] $PbBr_2$ and $CH_3NH_3Br$ were dissolved in DMF, followed by adding the toluene solution containing OLA and OA at room temperature, which acted as surfactants that stabilized the polar DMF phase in the nonpolar toluene phase. In addition, OLA weakly protonates OA to $OA^+$, which is required to limit the growth of NCs. The amount and ratio of long-chain molecules determine the thickness of 2D perovskites. This approach yields $CH_3NH_3PbBr_3$ NPLs with various $n$ values, with PL centered at 517, 489, 456, and 436 nm (Fig. 4e) corresponding to $n$ = 7–10, 5, 3, and 1, respectively. The high monodispersity and mild reaction conditions have led to high PLQYs (40–90%) in colloidal solutions. Interestingly, contrary to other protocols, the use of OLA and OA seems to enhance the colloidal stability of the synthesized NPLs.[75]

On the other hand, less research effort has been focused on the colloidal synthesis of 2D iodide perovskites. Hassan *et al.* developed a direct synthesis route of 2D $CH_3NH_3PbI_3$ NCs.[76] It is a two-step approach involving (i) the preparation of monodispersed $PbI_2$ NPL solution and (ii) reaction of the solution with a mixture containing alkyl ammonium iodide and methylammonium iodide. They found that the lateral size of $PbI_2$ seeds played a minor role in determining the resulting $n$. Depending on the ratios between the reactants, 2D $CH_3NH_3PbI_3$ colloidal dispersions with $n$ = 0, 1, and 2 were obtained, yielding green, orange, and red emissions, respectively. Weidman *et al.* studied the influence of halide composition on the photophysical properties of perovskite NPLs. Apart from the Br-based 2D perovskites, I-based counterparts were also prepared (with both $CH_3NH_3^+$ and $CH(NH_2)_2^+$).[74] However, the PLQYs are not satisfactory (<2%) and the NPLs with $n > 1$ were not reported. The Sn-based 2D perovskites were also reported, but the PLQYs remain low;[74] in particular, the entire process has to be carried out in an inert atmosphere due to the high reactivity with oxygen.[77] Another interesting approach was presented by Hintermayr *et al.* and Tong *et al.* by using a tip sonicator to disperse the bulk perovskite phase in a nonpolar solvent containing ligand molecules.[78,79] The same research group further found that the formation of 2D NPLs can also be triggered by diluting a solution containing thick NCs of $CH_3NH_3PbBr_3$ or $CH_3NH_3PbI_3$.[80] Note that although the thin 2D iodide counterparts could be formed using both methods mentioned above, there is a lack of selectivity toward precise layer control.

Colloidal-based methods have brought new opportunities for 2D perovskites in optoelectronics. Precise layering control from $n$ = 0 to $n$ = $\infty$ has been achieved in colloidal $CH_3NH_3PbBr_3$ and $CsPbBr_3$ perovskite systems. Moreover, it has been shown that the synthesis procedures commonly used for obtaining colloidal perovskite NCs can be readily scaled-up, thus potentially enabling the production on an industrial scale.[81–83] Nevertheless, most of the synthesis methods discussed in this section yield 2D bromide perovskite colloidal dispersions. Although the 2D confined structures have been proven to stabilize the cubic phase to some degree, it still remains challenging for $n > 2$. We believe that this is the fundamental mechanism responsible for the low yield in 2D iodide perovskites. In addition, for 2D perovskite NPL dispersions with $n < 3$, the PLQYs remain low. All the values of this parameter achieved for various colloidal dispersions of 2D perovskites are summarized in Table 3. We expect that further research effort will be focused on QY improvement.

Table 3 Summary of various 2D perovskite structures prepared by colloidal synthesis together with their photophysical properties

| Compound | Layer number $n$ | $\lambda_{Abs}$ (nm) | $\lambda_{PL}$ (nm) | PLQY (%) | Ref. |
|---|---|---|---|---|---|
| $CH_3NH_3PbBr_3$ | $\infty$ | 525 | 530 | — | 36 |
| | 6 | 497 | 504 | — | 36 |
| | 5 | 486 | 490 | — | 36 |
| | 4 | 472 | 475 | — | 36 |
| | 3 | 451 | — | — | 36 |
| | 1 | 431 | — | — | 36 |
| $CH_3NH_3PbBr_3$ | $\infty$ | 528 | 518 | 16 | 69 |
| | 5 | — | 490 | | 69 |
| | 4 | 463 | 469 | 12 | 69 |
| | 3 | 446 | 454 | 3 | 69 |
| | 0 | — | 427 | 0.4 | 69 |
| $CH_3NH_3PbBr_3$ | $\infty$ | — | 532 | 15 | 70 |
| | 3 | ~450 | 465 | 18 | 70 |
| $CH_3NH_3PbI_3$ | $\infty$ | — | ~700 | — | 70 |
| $CsPbBr_3$ | 5 | — | 488 | 84 | 71 |
| | 4 | — | 477 | 45 | 71 |
| | 3 | — | 462 | 10 | 71 |
| | 1 | — | 435 | — | 71 |
| | 0 | — | 405 | — | 71 |
| $CsPbBr_3$ | $\infty$ | — | 510 | 78 | 72 |
| | 4 | 441 | 459 | 31 | 73 |
| | 3 | 431 | 449 | — | 73 |
| | 2 | 422 | 438 | — | 73 |
| $CH_3NH_3PbBr_3$ | 1 | 348 | — | — | 74 |
| | 0 | 334 | — | — | 74 |
| $CH(NH_2)_2PbCl_3$ | 1 | 354 | — | — | 74 |
| $CH_3NH_3PbBr_3$ | 1 | 431 | 437 | 6 | 74 |
| | 0 | 398 | 403 | — | 74 |
| $CH(NH_2)_2PbBr_3$ | 1 | 434 | 439 | 22 | 74 |
| $CsPbBr_3$ | 1 | 429 | 433 | — | 74 |
| $CH_3NH_3PbBr_3$ | 1 | 566 | 574 | 1.1 | 74 |
| | 0 | 506 | 513 | — | 74 |
| $CH(NH_2)_2PbI_3$ | 1 | 566 | 575 | 1.4 | 74 |
| $CsPbI_3$ | 1 | 553 | 561 | — | 74 |
| $CH(NH_2)_2SnI_3$ | 1 | 674 | 689 | 2.6 | 74 |
| | 0 | 604 | 628 | 0.5 | 74 |
| $CH_3NH_3PbBr_3$ | 7–10 | ~511 | 517 | 81 | 68 |
| | 5 | 469 | 489 | 90 | 68 |
| | 3 | 449 | 456 | 50 | 68 |
| | 1 | 429 | 436 | 10 | 68 |
| $CH_3NH_3PbI_3$ | 2 | 593–600 | 610 | — | 76 |
| | 1 | 565 | 580 | — | 76 |
| | 0 | 505 | 520 | — | 76 |

# IV. Optoelectronic applications

Hybrid perovskites are an emerging class of semiconducting materials that have shown promising potential in the optoelectronic and photonic devices. In this section, we review

recent progress in 2D-perovskite-based optoelectronics, including LEDs, and solar cells.

### Light-emitting diodes

The first observation for EL of 2D perovskites was reported back in 1994.[84] The hybrid perovskite $(C_6H_5C_2H_4NH_3)_2PbI_4$ or $PEAPbI_4$ ($n = 0$) exhibited EL at ~520 nm with maximum luminance up to 10 000 cd $m^{-2}$ at liquid-nitrogen temperature. Room-temperature EL of perovskites ($n = \infty$) was reported two decades later using $CH_3NH_3PbI_{3-x}Cl_x$, $CH_3NH_3PbBr_3$, and $CH_3NH_3PbBr_2I$ polycrystalline films.[85] The NIR device showed the highest EQE of 0.76% and maximum radiance of 13.2 W $sr^{-1}$ $m^{-2}$ at 780 nm, and the green and red LEDs demonstrate the maximum EQEs of 0.1% and 0.018%, respectively. Since then, considerable research effort has been made to enhance the performance of perovskite LEDs. The emergence of perovskite emitters has opened an avenue toward low-cost and roll-to-roll fabrication of large-area optoelectronics due to the long radiative recombination lifetime,[86] high charge carrier motility,[87,88] fair PLQYs,[89–93] and the emission can be easily tuned from visible to infrared wavelengths.[33,74,94–96] Recently, a number of device architectures[97] have been proposed to enable high-performance perovskite LEDs.[98–117] With the fundamental background addressed in Section I in mind, we believe that layer-controlled 2D perovskites are the ultimate solution for high-performance perovskite LEDs.

The first report that demonstrates LED devices based on pure-inorganic $CsPbBr_3$ perovskite QDs has shown a few nanometers of blue shift, which might result from a small degree of quantum confinement effect as compared to that in the bulk $CsPbBr_3$ (~530 nm) counterpart.[118] The device structure with Au/MgNiO/$CsPbBr_3$ QDs/*n*-MgZnO/*n*-GaN demonstrates green emission at 522 nm with a maximum EQE of 2.39% and a maximum luminance of 3809 cd $m^{-2}$.[119] It also showed operational stability of 10 h, with only 20% drop in device efficiency. By controlling the surface density of ligands, the PLQY, colloidal solution stability, and carrier injection ability of the $CsPbBr_3$ perovskite QDs were found to be greatly enhanced.[120] The resulting devices showed the maximum luminance of 15185 cd $m^{-2}$ at 512 nm with a maximum EQE of 6.27% and a maximum current efficiency of 13.30 cd $A^{-1}$.[120] For the blue perovskite-based LEDs, an EQE of 0.07% at 455 nm was achieved with mixed halides $CsPbX_3$ perovskite QDs.[121] Indeed, it remains challenging to induce a sizable and controllable degree of quantum confinement in perovskite QDs. Despite the fact that the role of ligand type and their concentrations is one of the critical issues for colloidal stability and device performance, the role of organic ligands is beyond the scope of this review and may be addressed elsewhere.

Fig. 5 shows the device architectures and *I–V–L* characteristics of quasi-2D (layered structure of the 2D and 3D perovskites) perovskite emitters-based red and green LEDs. With the quasi-2D perovskites, it has been reported that a small amount of 1-naphthylmethylammonium lead tetra iodide ($(NMA)_2PbI_4$, $n = 0$) in the bulk $CH(NH_2)_2PbI_3$ perovskite matrix yields the maximum EQE of 11.70% and the highest radiance of 82 W $sr^{-1}$ $m^{-2}$, with the EL peak emission at 763 nm (Fig. 5a–c).[122] The LED devices using pure, layer-controlled quasi-2D ($n = 0$, 1, and 2) perovskites with multi-quantum wells (MQWs) structure were also demonstrated in the $(C_4H_9NH_3)_2[CH_3NH_3PbX_3]_nPbI_4$ system, with tunable EL peak position from 700 ($n = 2$) to 518 nm ($n = 0$).[123] For $n = 2$, the maximum EQE of 2.29% and maximum luminance of 214 cd $m^{-2}$ were demonstrated, while for the counterparts of $n = 1$ and 0, the EQEs were orders of magnitude lower.[123] Yuan *et al.* further reported the record high EQE of 8.8%, with the maximum radiance of 80 W $sr^{-1}$ $m^{-2}$ at 700 nm by using the mixed multilayered quasi-2D perovskites of $(C_6H_5C_2H_4NH_3)_2[CH_3NH_3PbI_3]_nPbI_4$ ($n$ = 0–3) (Fig. 5b).[124] They proposed that these high efficiencies result from the cascade energy transfer between the 2D layers, thereby promoting smooth charge injection, as well as effective exciton recombination.

Next, we move to the bromide perovskite compounds, which yield green to blue emissions (400–550 nm). Note that the performance of iodide-perovskites-based deep-red/NIR LEDs has not yet been achieved in bromide-based green/blue LED counterparts.[125] Upon mixing 2D $(C_6H_5C_2H_4NH_3)_2PbBr_4$ ($n = 0$) in the bulk $CH_3NH_3PbBr_3$ matrix, which is also known as quasi-2D perovskite, green LEDs (at 520 nm) with a high current efficiency of 4.90 cd $A^{-1}$ and maximum luminance of 2935 cd $m^{-2}$ have been demonstrated.[126] Wei *et al.* also reported the maximum EQE of 0.53% and current efficiency of 1.43 cd $A^{-1}$ using 2D $CH_3NH_3PbBr_3$ perovskites.[127] Recently, based on pure $(C_6H_5C_2H_4NH_3)_2PbBr_4$ ($n = 0$) NPLs, room-temperature violet LEDs emitting at 410 nm were reported.[128]

The relatively poor performance in NPLs-based devices may result from the electrical shunting between the electrodes, since the assembled 2D perovskite NPLs tend to be rough. This issue can be improved by incorporating NPLs in a low-dielectric-constant organic or polymer matrix.[68,129] Ling *et al.* reported the maximum luminance of 10 590 cd $m^{-2}$ using $CH_3NH_3PbBr_3$ NPL films reinforced in an ambipolar mixture of PVK:PBD host,[130] although the device EQE remains low (0.38%). Fig. 5e–h show the architecture, *I–V–L* characteristics, and EL spectra (at different driving voltages) of 2D $CH_3NH_3PbBr_3$ perovskite LEDs. Very recently, our group demonstrated efficient 2D $CH_3NH_3PbBr_3$ perovskite devices using the low-dielectric-constant, fluorescent host materials, which enables the Förster resonance energy transfer (FRET) between the host and 2D perovskites (Fig. 6a and d).[68] By using quantum-confined 2D $CH_3NH_3PbBr_3$ emitters with $n = 1$ (deep-blue), $n = 3$ (pure blue), $n = 5$ (cyan), and $n = 7$–10 (green), EQEs ranging from 2.31% to 0.004% have been demonstrated. The EL spectra, device architecture, and energy levels of materials are presented in Fig. 6b and c. In order to further enhance the performance of 2D perovskite-based LEDs, we expect that a deeper understanding in efficient energy transfer between perovskite and organic materials would be essential.

### Solar cells

Since the first demonstration of organometal halide perovskite (OHP) as a photosensitizer in the dye-sensitized solar cell (DSSC) by Miyasaka group in 2009,[131] considerable attention has been drawn toward the development of perovskite solar cells to address the issues of low power conversion efficiency

 

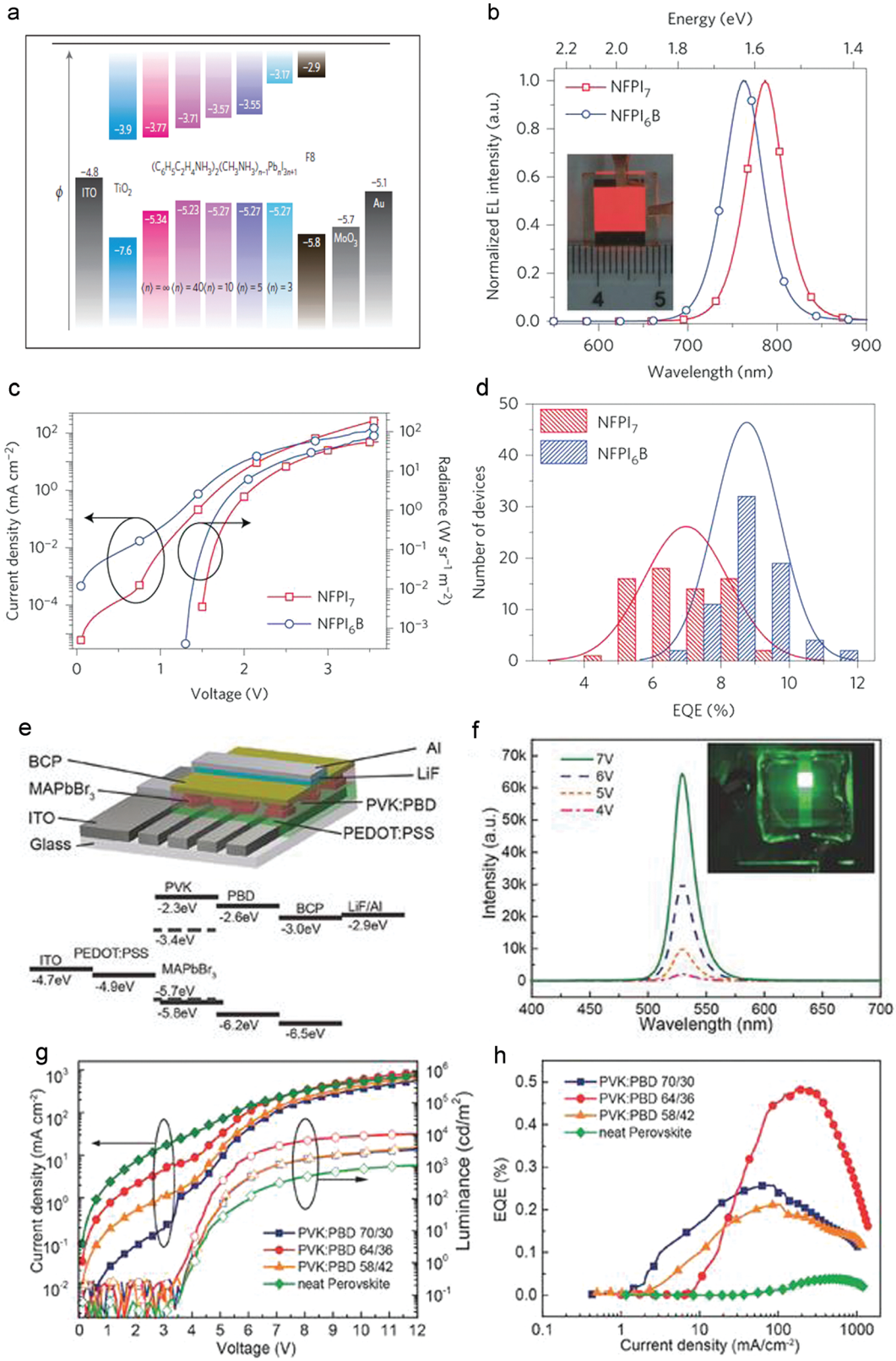


Fig. 5 (a) Schematic diagram of the energy levels of the 2D perovskite with different *n* values, carrier transporting materials $TiO_2$ with electrodes, ITO and Au. Reproduced with permission. Copyright 2016, Macmillan Publishers Limited.[124] (b) EL spectra of the devices under 3 V. Inset: Photograph of a 0.64 $cm^2$ $NFPI_6B$ device.[122] (c) Current density *vs.* voltage *vs.* radiance of LED devices using $FPI_7$ and $NFPI_6Br$.[122] (d) Histograms of peak EQEs measured from 67 $NFPI_7$ and 70 $NFPI_6B$ devices. (b–d) Reproduced with permission. Copyright 2016, Macmillan Publishers Limited.[122] (e) Device architecture and energy levels of all materials.[130] (f) EL spectra of LED at different operation voltages. Inset, photograph of green LED using layered 2D perovskite of $MAPbBr_3$.[130] (g) *J*–*V*–*L* characteristics[130] and (h) EQE *vs.* *J* for the devices. (e–h) Reproduced with permission. Copyright 2016, Wiley-VCH.[130]

(PCE), poor device stability, and dubious reproducibility. In 2011, Park's group improved the PCE to 6.54% by using $MAPbI_3$ QD photosensitizers.[132] The "*perovskite fever*"[133,134] rose in 2013, after Park's group reported a PCE of 9.7% by using the solid-state hole transport material (HTM), spiro-OMeTAD.[135] The resulting solar cells exhibited long-term stability of over 500 hours under ambient conditions. At the same time, the PCE is further enhanced to 10.9% as mesoporous $Al_2O_3$ was employed to replace the $TiO_2$ layer.[136] In July 2013, Grätzel and co-workers demonstrated a high PCE of ~15% by sequentially depositing $PbI_2$ and $CH_3NH_3I$ precursors onto the mesoporous $TiO_2$ layer.[137] In these methods, the slow diffusion of $CH_3NH_3I$ solution in the $PbI_2$ lattice matrix was considered to be the main challenge to achieve defect-free and homogenous perovskite films. To this end, Snaith's group used dual-source thermal evaporation to prepare the mixed halide perovskite $CH_3NH_3PbI_{3-x}Cl_x$ and achieved a PCE of 15.4% in the planar heterojunction structure.[138] Recently, PCEs of 19.3, 20.1, and 21.1% were achieved by the Yang group (2014),[139] Seok group (2015),[140] and Grätzel group (2016),[141] respectively. Up to now, within only 7 years, perovskite solar cells have reached a record-high PCE of 22.1%,[142] comparable to that of silicon-based solar cells.

It has been well recognized that the most significant challenge toward the commercialization of perovskite solar cells is device stability under continuous illumination at elevated temperatures.[143–146] This motivates the development of 2D- and quasi-2D-perovskites-based solar cells.[147,148] In 2014, by incorporating 2D $(C_6H_5C_2H_4NH_3)_2(CH_3NH_3)_2Pb_3I_{10}$ ($n$ = 2) light absorber into bulk $CH_3NH_3PbI_3$, Smith *et al.* demonstrated the hybrid perovskite solar cell with a PCE of 4.73% and an open circuit voltage of 1.18 V.[59] The 2D perovskites have shown better resistance from moisture as compared to bulk $CH_3NH_3PbI_3$. Likewise, the maximum PCE of ~4% has been attained for the layered 2D $(C_4H_9NH_3)_2[CH_3NH_3PbX_3]_nPbI_4$ ($n$ = 0, 1, 2, and 3) perovskites-based solar cells.[50] The transport barriers between layers in the 2D perovskite systems appear to be the major mechanism responsible for the reduction of PCE,[149] as well as a high open circuit voltage.[150] A higher PCE of 8.5% was realized by using a mixture of 2D and 3D $(C_6H_5C_2H_4NH_3)_2[CH_3NH_3PbX_3]_nPbI_4$, with $n$ = 1, 2, 3, up to $\infty$.[150] The Sargent group realized a PCE of 15.3% using the same material system, with $n$ = 60 and $n$ = 40.[151] Under high relative humidity of 55%, the PCE only showed a ~10% drop after 60 day (1440 hour) operation.[151] The Mohite group also reported a high PCE of 12.52% using a mixture containing bilayer ($n$ = 2) and trilayer ($n$ = 3) $(C_4H_9NH_3)_2[CH_3NH_3PbX_3]_nPbI_4$ perovskites along with retaining 60% of the initial PCE after 2250 hour operation under ambient conditions (Fig. 7a and b).[63] Another report that used a mixed 2D $(HOOC(CH_2)_2NH_3)_2PbI_4$ ($n$ = 0) and 3D $MAPbI_3$ light absorber also achieved a PCE of 11.2% as well as a 5000 hour-long ambient stability.[152] Clearly, after incorporating 2D perovskites into the light absorber, the trade-off between the PCE decrease

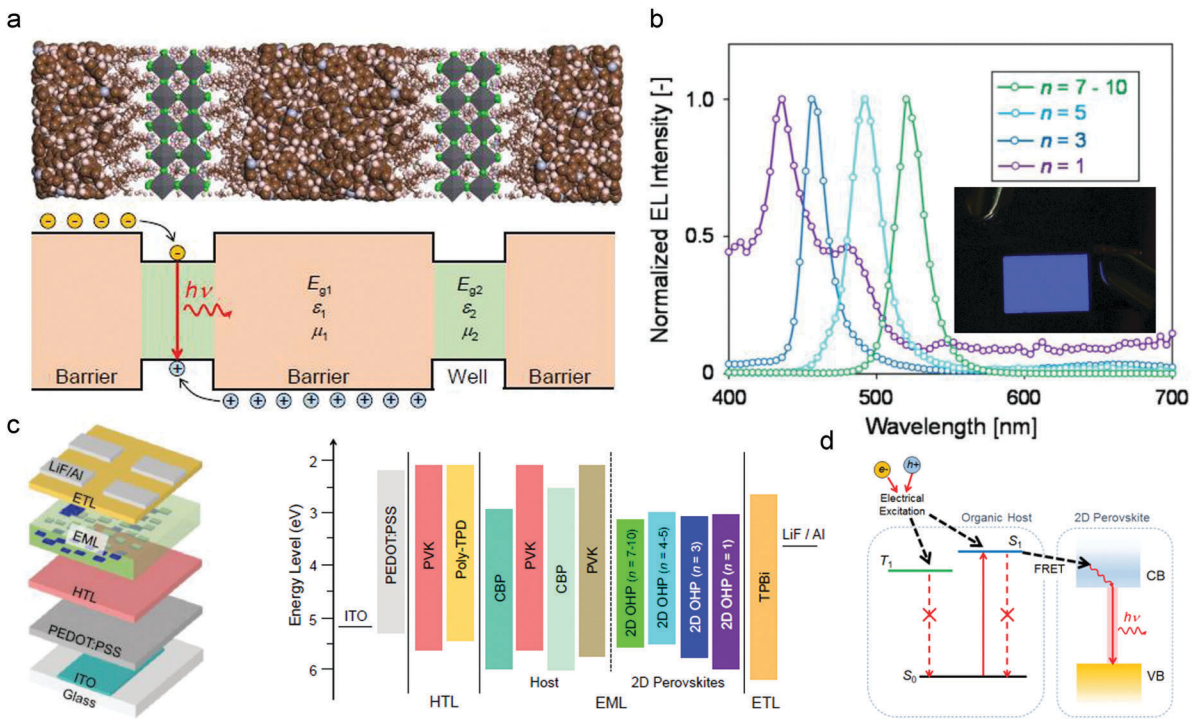


Fig. 6 (a) Schematic (bottom) and molecular model (top) of the dielectric quantum wells formed between organic host molecules (barriers, 1) and 2D perovskites (wells, 2), illustrating $E_{g1} > E_{g2}$, $\varepsilon_1 < \varepsilon_2$, and $\mu_1 > \mu_2$ to enhance $E_B$ in the wells.[68] (b) LED device architecture and energy level diagram of materials.[68] (c) Representative EL spectra for LEDs using colloidal solutions of $n$ = 7–10 (pure green), $n$ = 5 (sky blue), $n$ = 3 (pure blue), and $n$ = 1 (deep blue), Inset: Photograph of a pure-blue LED (area: 3 × 5 $mm^2$).[68] (d) Schematic of FRET occurring at the interface between organic host and 2D perovskite, in which the singlet excitons in the host transferred to the conduction band (CB) in 2D perovskite.[68] (a–d) Reproduced with permission. Copyright 2016, American Chemical Society.[68]

 

and stability enhancement represents the major challenge in this field.

### Other applications

Lead halide perovskites have also been demonstrated for other optoelectronic applications, such as photo-field effect transistors,[153] color convertors,[154] and waveguides.[155,156] In particular, perovskite-based photodetectors to detect visible,[157] X-rays,[158,159] UV,[160] and γ-ray photons[161] have been reported. However, only a few reports have addressed these applications using 2D perovskites. Here, we briefly review the relevant literature. Liu and co-workers reported a photodetector comprising 2D $CH_3NH_3PbI_3$ perovskite NPLs (Fig. 7c). It showed a high value of photoresponsivity up to 21 mA $W^{-1}$, which is significantly improved as compared to those based on bulk $CsPbBr_3$ and $CH_3NH_3PbI_3$.[162] Another report also demonstrated 2D-perovskite-based photodetectors using $(C_4H_9NH_3)_2[CH_3NH_3PbX_3]_nPbI_4$, showing photoconductivity values of 3.0 ($n$ = 0), 7.31 ($n$ = 1), and 12.78 ($n$ = 2) mA $W^{-1}$.[163,164] Ahmad *et al.* also observed a high photocurrent by using a 2D perovskite film comprising $(C_6H_5C_2H_4NH_3)_2PbI_4$ ($n$ = 0).[165] The photodetectors based on inorganic 2D $CsPbX_3$ perovskite NPLs also exhibited high on/off ratios and fast response time (Fig. 7d).[166]

## V. Summary

Layer-controlled 2D hybrid perovskites represent one of the very few semiconductor systems that allow tailoring of the optoelectronic properties by means of $n$, bridging the materials synthesis with the physics of semiconductor quantum wells developed in the 1990s. In combination with their appropriate bandgaps that covers the entire visible wavelength region, we expect that the scientific and engineering challenges and opportunities addressed in this review will greatly facilitate the development of perovskite-based optoelectronic devices.

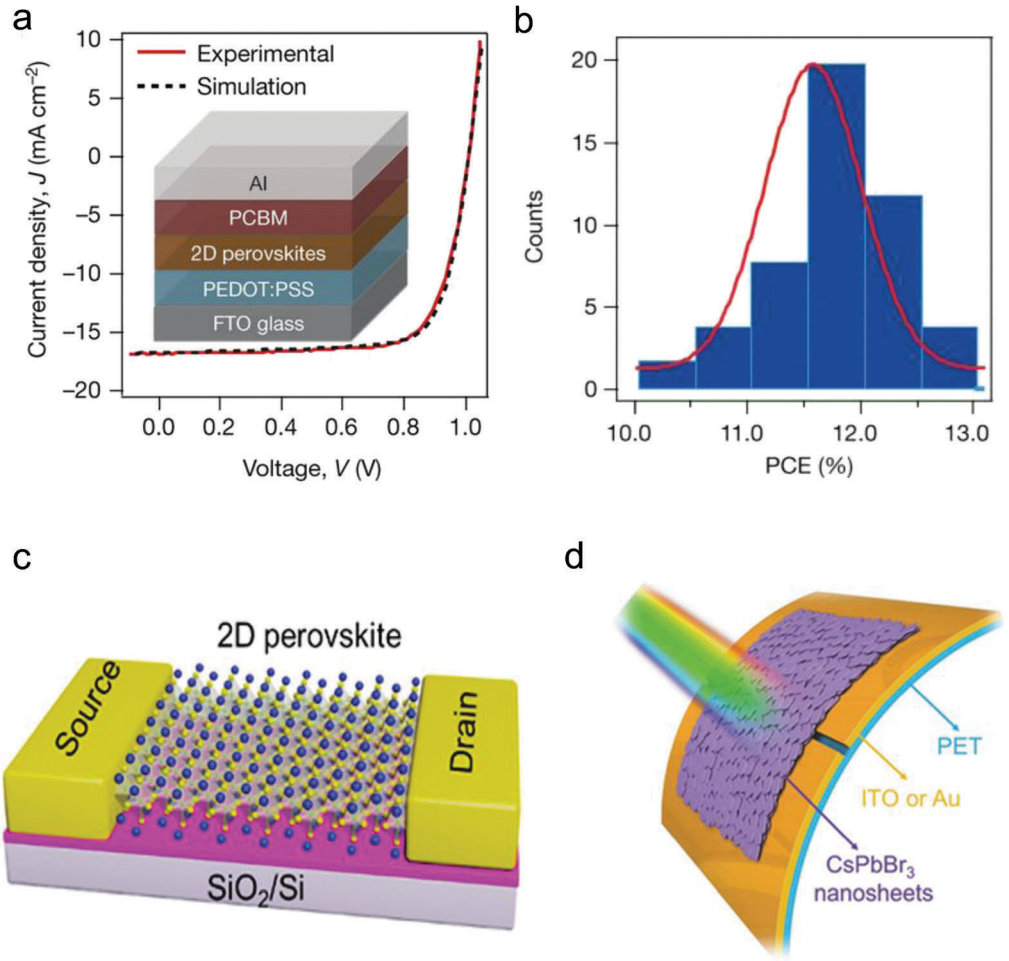


Fig. 7 (a) $J$–$V$ characteristics of planar devices using 2D $(BA)_2(MA)_3Pb_4I_{13}$ perovskites, Inset-device architecture consisting 2D $(BA)_2(MA)_3Pb_4I_{13}$ perovskites light absorber.[63] (b) Histogram of $(BA)_2(MA)_3Pb_4I_{13}$ device power conversion efficiency (PCE) over 50 measured devices, fitted with a Gaussian distribution.[63] (a and b) Reproduced with permission. Copyright 2016, Macmillan Publishers Limited.[63] (c) Schematic device architecture of photodetector with 2D $CH_3NH_3PbI_3$ perovskite.[48] Reproduced with permission. Copyright 2016, American Chemical Society.[48] (d) Schematic device architecture of flexible photodetector using 2D $CsPbBr_3$ perovskite nanosheets.[162] Reproduced with permission. Copyright 2016, Wiley-VCH.[162]

## Acknowledgements

The authors are grateful for financial support from ETH startup funding.

## References

1 H. L. Wells, *Z. Anorg. Chem.*, 1893, **3**, 195–210.
2 C. K. Moller, *Nature*, 1958, **182**, 1436.
3 J. S. Manser, J. A. Christians and P. V. Kamat, *Chem. Rev.*, 2016, **116**, 12956–13008.
4 B. Saparov and D. B. Mitzi, *Chem. Rev.*, 2016, **116**, 4558–4596.
5 C. Li, X. Lu, W. Ding, L. Feng, Y. Gao and Z. Guo, *Acta Crystallogr., Sect. B: Struct. Sci.*, 2008, **64**, 702–707.
6 M. A. Green, A. Ho-Baillie and H. J. Snaith, *Nat. Photonics*, 2014, **8**, 506–514.
7 R. J. Ellingson, M. C. Beard, J. C. Johnson, P. Yu, O. I. Micic, A. J. Nozik, A. Shabaev and A. L. Efros, *Nano Lett.*, 2005, **5**, 865–871.
8 V. D'Innocenzo, G. Grancini, M. J. P. Alcocer, A. R. S. Kandada, S. D. Stranks, M. M. Lee, G. Lanzani, H. J. Snaith and A. Petrozza, *Nat. Commun.*, 2014, **5**, 3586.
9 J. Even, L. Pedesseau and C. Katan, *J. Phys. Chem. C*, 2014, **118**, 11566–11572.
10 E. J. Juarez-Perez, R. S. Sanchez, L. Badia, G. Garcia-Belmonte, Y. S. Kang, I. Mora-Sero and J. Bisquert, *J. Phys. Lett.*, 2014, **5**, 2390–2394.
11 Q. Lin, A. Armin, R. C. R. Nagiri, P. L. Burn and P. Meredith, *Nat. Photonics*, 2015, **9**, 106–112.
12 Y. Yamada, T. Nakamura, M. Endo, A. Wakamiya and Y. Kanemitsu, *IEEE J. Photovolt.*, 2015, **5**, 401–405.
13 A. Miyata, A. Mitioglu, P. Plochocka, O. Portugall, J. T.-W. Wang, S. D. Stranks, H. J. Snaith and R. J. Nicholas, *Nat. Phys.*, 2015, **11**, 582–587.
14 L. M. Herz, *Annu. Rev. Phys. Chem.*, 2016, **67**, 65–89.
15 J. M. Frost and A. Walsh, *Acc. Chem. Res.*, 2016, **49**, 528–535.
16 A. Pecchia, D. Gentilini, D. Rossi, M. Auf der Maur and A. Di Carlo, *Nano Lett.*, 2016, **16**, 988–992.
17 C. Motta, F. El-Mellouhi, S. Kais, N. Tabet, F. Alharbi and S. Sanvito, *Nat. Commun.*, 2015, **6**, 7026.
18 T. Etienne, E. Mosconi and F. De Angelis, *J. Phys. Lett.*, 2016, **7**, 1638–1645.
19 F. Zheng, L. Z. Tan, S. Liu and A. M. Rappe, *Nano Lett.*, 2015, **15**, 7794–7800.
20 H. Zhu, K. Miyata, Y. Fu, J. Wang, P. P. Joshi, D. Niesner, K. W. Williams, S. Jin and X.-Y. Zhu, *Science*, 2016, **353**, 1409–1413.
21 O. D. Miller, E. Yablonovitch and S. R. Kurtz, *IEEE J. Photovolt.*, 2012, **2**, 303–311.
22 H.-S. Kim, S. H. Im and N.-G. Park, *J. Phys. Chem. C*, 2014, **118**, 5615–5625.
23 S. D. Stranks and H. J. Snaith, *Nat. Nanotechnol.*, 2015, **10**, 391–402.
24 B. R. Sutherland and E. H. Sargent, *Nat. Photonics*, 2016, **10**, 295–302.
25 S. Reineke, M. Thomschke, B. Lüssem and K. Leo, *Rev. Mod. Phys.*, 2013, **85**, 1245–1293.
26 Y. Shirasaki, G. J. Supran, M. G. Bawendi and V. Bulovic, *Nat. Photonics*, 2013, **7**, 13–23.
27 C. Zhang, D. Sun, C. X. Sheng, Y. X. Zhai, K. Mielczarek, A. Zakhidov and Z. V. Vardeny, *Nat. Phys.*, 2015, **11**, 427–434.
28 E. Edri, S. Kirmayer, S. Mukhopadhyay, K. Gartsman, G. Hodes and D. Cahen, *Nat. Commun.*, 2014, **5**, 3461.
29 H. Cho, S.-H. Jeong, M.-H. Park, Y.-H. Kim, C. Wolf, C.-L. Lee, J. H. Heo, A. Sadhanala, N. Myoung, S. Yoo, S. H. Im, R. H. Friend and T.-W. Lee, *Science*, 2015, **350**, 1222–1225.
30 V. D'Innocenzo, A. R. Srimath Kandada, M. De Bastiani, M. Gandini and A. Petrozza, *J. Am. Chem. Soc.*, 2014, **136**, 17730–17733.
31 A. Sadhanala, S. Ahmad, B. Zhao, N. Giesbrecht, P. M. Pearce, F. Deschler, R. L. Z. Hoye, K. C. Gödel, T. Bein, P. Docampo, S. E. Dutton, M. F. L. De Volder and R. H. Friend, *Nano Lett.*, 2015, **15**, 6095–6101.
32 K. Zheng, Q. Zhu, M. Abdellah, M. E. Messing, W. Zhang, A. Generalov, Y. Niu, L. Ribaud, S. E. Canton and T. Pullerits, *J. Phys. Lett.*, 2015, **6**, 2969–2975.
33 L. Protesescu, S. Yakunin, M. I. Bodnarchuk, F. Krieg, R. Caputo, C. H. Hendon, R. X. Yang, A. Walsh and M. V. Kovalenko, *Nano Lett.*, 2015, **15**, 3692–3696.
34 K. Tanaka, T. Takahashi, T. Ban, T. Kondo, K. Uchida and N. Miura, *Solid State Commun.*, 2003, **127**, 619–623.
35 I. B. Koutselas, L. Ducasse and G. C. Papavassiliou, *J. Phys.: Condens. Matter*, 1996, **8**, 1217.
36 P. Tyagi, S. M. Arveson and W. A. Tisdale, *J. Phys. Lett.*, 2015, **6**, 1911–1916.
37 G. Bastard, E. E. Mendez, L. L. Chang and L. Esaki, *Phys. Rev. B: Condens. Matter Mater. Phys.*, 1982, **26**, 1974–1979.
38 T. Ishihara, J. Takahashi and T. Goto, *Phys. Rev. B: Condens. Matter Mater. Phys.*, 1990, **42**, 11099–11107.
39 M. Kumagai and T. Takagahara, *Phys. Rev. B: Condens. Matter Mater. Phys.*, 1989, **40**, 12359–12381.
40 K. Tanaka, T. Takahashi, T. Kondo, T. Umebayashi, K. Asai and K. Ema, *Phys. Rev. B: Condens. Matter Mater. Phys.*, 2005, **71**, 045312.
41 H. Huang, L. Polavarapu, J. A. Sichert, A. S. Susha, A. S. Urban and A. L. Rogach, *NPG Asia Mater.*, 2016, **8**, e328.
42 S.-T. Ha, R. Su, J. Xing, Q. Zhang and Q. Xiong, *Chem. Sci.*, 2017, **8**, 2522–2536.
43 M. Sessolo, L. Gil-Escrig, G. Longo and H. J. Bolink, *Top. Curr. Chem.*, 2016, **374**, 52.
44 S. T. Ha, X. F. Liu, Q. Zhang, D. Giovanni, T. C. Sum and Q. H. Xiong, *Adv. Opt. Mater.*, 2014, **2**, 838–844.
45 S. Z. Butler, S. M. Hollen, L. Cao, Y. Cui, J. A. Gupta, H. R. Gutiérrez, T. F. Heinz, S. S. Hong, J. Huang, A. F. Ismach, E. Johnston-Halperin, M. Kuno, V. V. Plashnitsa, R. D. Robinson, R. S. Ruoff, S. Salahuddin, J. Shan, L. Shi, M. G. Spencer, M. Terrones, W. Windl and J. E. Goldberger, *ACS Nano*, 2013, **7**, 2898–2926.
46 L. Niu, X. F. Liu, C. X. Cong, C. Y. Wu, D. Wu, T. R. Chang, H. Wang, Q. S. Zeng, J. D. Zhou, X. L. Wang, W. Fu, P. Yu,

 

Q. D. Fu, S. Najmaei, Z. H. Zhang, B. I. Yakobson, B. K. Tay, W. Zhou, H. T. Jeng, H. Lin, T. C. Sum, C. Jin, H. Y. He, T. Yu and Z. Liu, *Adv. Mater.*, 2015, **27**, 7800–7808.
47 Y. P. Wang, Y. F. Shi, G. Q. Xin, J. Lian and J. Shi, *Cryst. Growth Des.*, 2015, **15**, 4741–4749.
48 J. Y. Liu, Y. Z. Xue, Z. Y. Wang, Z. Q. Xu, C. X. Zheng, B. Weber, J. C. Song, Y. S. Wang, Y. R. Lu, Y. P. Zhang and Q. L. Bao, *ACS Nano*, 2016, **10**, 3536–3542.
49 G. Wang, D. Li, H.-C. Cheng, Y. Li, C.-Y. Chen, A. Yin, Z. Zhao, Z. Lin, H. Wu, Q. He, M. Ding, Y. Liu, Y. Huang and X. Duan, *Sci. Adv.*, 2015, **1**, e1500613.
50 D. H. Cao, C. C. Stoumpos, O. K. Farha, J. T. Hupp and M. G. Kanatzidis, *J. Am. Chem. Soc.*, 2015, **137**, 7843–7850.
51 C. C. Stoumpos, D. H. Cao, D. J. Clark, J. Young, J. M. Rondinelli, J. I. Jang, J. T. Hupp and M. G. Kanatzidis, *Chem. Mater.*, 2016, **28**, 2852–2867.
52 T. Ishihara, J. Takahashi and T. Goto, *Solid State Commun.*, 1989, **69**, 933–936.
53 K. Tanaka and T. Kondo, *Sci. Technol. Adv. Mater.*, 2003, **4**, 599–604.
54 X. Hong, T. Ishihara and A. V. Nurmikko, *Phys. Rev. B: Condens. Matter Mater. Phys.*, 1992, **45**, 6961–6964.
55 T. Ishihara, *J. Lumin.*, 1994, **60-1**, 269–274.
56 T. Ishihara, in *Optical Properties of Low–Dimensional Materials*, ed. T. Ogawa and Y. Kanemitsu, World Scientific, 1995, pp. 288–339, DOI: 10.1142/9789814261388_0006.
57 J. Calabrese, N. L. Jones, R. L. Harlow, N. Herron, D. L. Thorn and Y. Wang, *J. Am. Chem. Soc.*, 1991, **113**, 2328–2330.
58 Y. Tabuchi, K. Asai, M. Rikukawa, K. Sanui and K. Ishigure, *J. Phys. Chem. Solids*, 2000, **61**, 837–845.
59 I. C. Smith, E. T. Hoke, D. Solis-Ibarra, M. D. McGehee and H. I. Karunadasa, *Angew. Chem., Int. Ed.*, 2014, **53**, 11232–11235.
60 D. B. Mitzi, *Chem. Mater.*, 1996, **8**, 791–800.
61 X. X. Wu, M. T. Trinh, D. Niesner, H. M. Zhu, Z. Norman, J. S. Owen, O. Yaffe, B. J. Kudisch and X. Y. Zhu, *J. Am. Chem. Soc.*, 2015, **137**, 2089–2096.
62 Z. Guo, X. X. Wu, T. Zhu, X. Y. Zhu and L. B. Huang, *ACS Nano*, 2016, **10**, 9992–9998.
63 H. H. Tsai, W. Y. Nie, J. C. Blancon, C. C. S. Toumpos, R. Asadpour, B. Harutyunyan, A. J. Neukirch, R. Verduzco, J. J. Crochet, S. Tretiak, L. Pedesseau, J. Even, M. A. Alam, G. Gupta, J. Lou, P. M. Ajayan, M. J. Bedzyk, M. G. Kanatzidis and A. D. Mohite, *Nature*, 2016, **536**, 312–316.
64 L. T. Dou, A. B. Wong, Y. Yu, M. L. Lai, N. Kornienko, S. W. Eaton, A. Fu, C. G. Bischak, J. Ma, T. N. Ding, N. S. Ginsberg, L. W. Wang, A. P. Alivisatos and P. D. Yang, *Science*, 2015, **349**, 1518–1521.
65 K. Gauthron, J. S. Lauret, L. Doyennette, G. Lanty, A. Al Choueiry, S. J. Zhang, A. Brehier, L. Largeau, O. Mauguin, J. Bloch and E. Deleporte, *Opt. Express*, 2010, **18**, 5912–5919.
66 L. C. Schmidt, A. Pertegás, S. González-Carrero, O. Malinkiewicz, S. Agouram, G. Mínguez Espallargas, H. J. Bolink, R. E. Galian and J. Pérez-Prieto, *J. Am. Chem. Soc.*, 2014, **136**, 850–853.
67 S. Gonzalez-Carrero, R. E. Galian and J. Perez-Prieto, *J. Mater. Chem. A*, 2015, **3**, 9187–9193.
68 S. Kumar, J. Jagielski, S. Yakunin, P. Rice, Y.-C. Chiu, M. Wang, G. Nedelcu, Y. Kim, S. Lin, E. J. G. Santos, M. V. Kovalenko and C.-J. Shih, *ACS Nano*, 2016, **10**, 9720–9729.
69 J. A. Sichert, Y. Tong, N. Mutz, M. Vollmer, S. Fischer, K. Z. Milowska, R. García Cortadella, B. Nickel, C. Cardenas-Daw, J. K. Stolarczyk, A. S. Urban and J. Feldmann, *Nano Lett.*, 2015, **15**, 6521–6527.
70 O. Vybornyi, S. Yakunin and M. V. Kovalenko, *Nanoscale*, 2016, **8**, 6278–6283.
71 Y. Bekenstein, B. A. Koscher, S. W. Eaton, P. Yang and A. P. Alivisatos, *J. Am. Chem. Soc.*, 2015, **137**, 16008–16011.
72 Q. A. Akkerman, V. D'Innocenzo, S. Accornero, A. Scarpellini, A. Petrozza, M. Prato and L. Manna, *J. Am. Chem. Soc.*, 2015, **137**, 10276–10281.
73 Q. A. Akkerman, S. G. Motti, A. R. Srimath Kandada, E. Mosconi, V. D'Innocenzo, G. Bertoni, S. Marras, B. A. Kamino, L. Miranda, F. De Angelis, A. Petrozza, M. Prato and L. Manna, *J. Am. Chem. Soc.*, 2016, **138**, 1010–1016.
74 M. C. Weidman, M. Seitz, S. D. Stranks and W. A. Tisdale, *ACS Nano*, 2016, **10**, 7830–7839.
75 J. De Roo, M. Ibáñez, P. Geiregat, G. Nedelcu, W. Walravens, J. Maes, J. C. Martins, I. Van Driessche, M. V. Kovalenko and Z. Hens, *ACS Nano*, 2016, **10**, 2071–2081.
76 Y. Hassan, Y. Song, R. D. Pensack, A. I. Abdelrahman, Y. Kobayashi, M. A. Winnik and G. D. Scholes, *Adv. Mater.*, 2016, **28**, 566–573.
77 P. Umari, E. Mosconi and F. De Angelis, *Sci. Rep.*, 2014, **4**, 4467.
78 V. A. Hintermayr, A. F. Richter, F. Ehrat, M. Döblinger, W. Vanderlinden, J. A. Sichert, Y. Tong, L. Polavarapu, J. Feldmann and A. S. Urban, *Adv. Mater.*, 2016, **28**, 9478–9485.
79 Y. Tong, E. Bladt, M. F. Aygüler, A. Manzi, K. Z. Milowska, V. A. Hintermayr, P. Docampo, S. Bals, A. S. Urban, L. Polavarapu and J. Feldmann, *Angew. Chem., Int. Ed.*, 2016, **55**, 13887–13892.
80 Y. Tong, F. Ehrat, W. Vanderlinden, C. Cardenas-Daw, J. K. Stolarczyk, L. Polavarapu and A. S. Urban, *ACS Nano*, 2016, **10**, 10936–10944.
81 K.-H. Wang, L. Wu, L. Li, H.-B. Yao, H.-S. Qian and S.-H. Yu, *Angew. Chem., Int. Ed.*, 2016, **55**, 8328–8332.
82 S. Wei, Y. Yang, X. Kang, L. Wang, L. Huang and D. Pan, *Chem. Commun.*, 2016, **52**, 7265–7268.
83 M. Yarema, O. Yarema, W. M. M. Lin, S. Volk, N. Yazdani, D. Bozyigit and V. Wood, *Chem. Mater.*, 2017, **29**, 796–803.
84 M. Era, S. Morimoto, T. Tsutsui and S. Saito, *Appl. Phys. Lett.*, 1994, **65**, 676–678.
85 Z. K. Tan, R. S. Moghaddam, M. L. Lai, P. Docampo, R. Higler, F. Deschler, M. Price, A. Sadhanala, L. M. Pazos, D. Credgington, F. Hanusch, T. Bein, H. J. Snaith and R. H. Friend, *Nat. Nanotechnol.*, 2014, **9**, 687–692.
86 S. D. Stranks, G. E. Eperon, G. Grancini, C. Menelaou, M. J. P. Alcocer, T. Leijtens, L. M. Herz, A. Petrozza and H. J. Snaith, *Science*, 2013, **342**, 341–344.
87 G. C. Xing, N. Mathews, S. Y. Sun, S. S. Lim, Y. M. Lam, M. Gratzel, S. Mhaisalkar and T. C. Sum, *Science*, 2013, **342**, 344–347.

88 Q. F. Dong, Y. J. Fang, Y. C. Shao, P. Mulligan, J. Qiu, L. Cao and J. S. Huang, *Science*, 2015, **347**, 967–970.
89 F. Deschler, M. Price, S. Pathak, L. E. Klintberg, D. D. Jarausch, R. Higler, S. Huttner, T. Leijtens, S. D. Stranks, H. J. Snaith, M. Atature, R. T. Phillips and R. H. Friend, *J. Phys. Chem. Lett.*, 2014, **5**, 1421–1426.
90 C. M. Sutter-Fella, Y. B. Li, M. Amani, J. W. Ager, F. M. Toma, E. Yablonovitch, I. D. Sharp and A. Javey, *Nano Lett.*, 2016, **16**, 800–806.
91 L. Martinez-Sarti, T. M. Koh, M. G. La-Placa, P. P. Boix, M. Sessolo, S. G. Mhaisalkar and H. J. Bolink, *Chem. Commun.*, 2016, **52**, 11351–11354.
92 H. Huang, A. S. Susha, S. V. Kershaw, T. F. Hung and A. L. Rogach, *Adv. Sci.*, 2015, **2**, 1500194.
93 X. M. Li, Y. Wu, S. L. Zhang, B. Cai, Y. Gu, J. Z. Song and H. B. Zeng, *Adv. Funct. Mater.*, 2016, **26**, 2435–2445.
94 S. Pathak, N. Sakai, F. W. R. Rivarola, S. D. Stranks, J. W. Liu, G. E. Eperon, C. Ducati, K. Wojciechowski, J. T. Griffiths, A. A. Haghighirad, A. Pellaroque, R. H. Friend and H. J. Snaith, *Chem. Mater.*, 2015, **27**, 8066–8075.
95 G. Nedelcu, L. Protesescu, S. Yakunin, M. I. Bodnarchuk, M. J. Grotevent and M. V. Kovalenko, *Nano Lett.*, 2015, **15**, 5635–5640.
96 M. L. Lai, T. Y. S. Tay, A. Sadhanala, S. E. Dutton, G. Li, R. H. Friend and Z.-K. Tan, *J. Phys. Chem. Lett.*, 2016, **7**, 2653–2658.
97 J. H. Jou, S. Kumar, A. Agrawal, T. H. Li and S. Sahoo, *J. Mater. Chem. C*, 2015, **3**, 2974–3002.
98 B. R. Sutherland and E. H. Sargent, *Nat. Photonics*, 2016, **10**, 295–302.
99 P. Kumar, B. Zhao, R. H. Friend, A. Sadhanala and K. S. Narayan, *ACS Energy Lett.*, 2017, **2**, 81–87.
100 Y.-H. Kim, H. Cho, J. H. Heo, T.-S. Kim, N. Myoung, C.-L. Lee, S. H. Im and T.-W. Lee, *Adv. Mater.*, 2015, **27**, 1248–1254.
101 S. G. R. Bade, J. Q. Li, X. Shan, Y. C. Ling, Y. Tian, T. Dilbeck, T. Besara, T. Geske, H. W. Gao, B. W. Ma, K. Hanson, T. Siegrist, C. Y. Xu and Z. B. Yu, *ACS Nano*, 2016, **10**, 1795–1801.
102 N. K. Kumawat, A. Dey, A. Kumar, S. P. Gopinathan, K. L. Narasimhan and D. Kabra, *ACS Appl. Mater. Interfaces*, 2015, **7**, 13119–13124.
103 W. L. Hong, Y. C. Huang, C. Y. Chang, Z. C. Zhang, H. R. Tsai, N. Y. Chang and Y. C. Chao, *Adv. Mater.*, 2016, **28**, 8029–8036.
104 A. Sadhanala, A. Kumar, S. Pathak, A. Rao, U. Steiner, N. C. Greenham, H. J. Snaith and R. H. Friend, *Adv. Electron. Mater.*, 2015, **1**, 1500008.
105 R. L. Z. Hoye, M. R. Chua, K. P. Musselman, G. Li, M.-L. Lai, Z.-K. Tan, N. C. Greenham, J. L. MacManus-Driscoll, R. H. Friend and D. Credgington, *Adv. Mater.*, 2015, **27**, 1414–1419.
106 J. P. Wang, N. N. Wang, Y. Z. Jin, J. J. Si, Z. K. Tan, H. Du, L. Cheng, X. L. Dai, S. Bai, H. P. He, Z. Z. Ye, M. L. Lai, R. H. Friend and W. Huang, *Adv. Mater.*, 2015, **27**, 2311–2316.
107 J. C. Yu, D. B. Kim, G. Baek, B. R. Lee, E. D. Jung, S. Lee, J. H. Chu, D. K. Lee, K. J. Choi, S. Cho and M. H. Song, *Adv. Mater.*, 2015, **27**, 3492–3500.
108 J. Q. Li, S. G. R. Bade, X. Shan and Z. B. Yu, *Adv. Mater.*, 2015, **27**, 5196–5202.
109 O. A. Jaramillo-Quintero, R. S. Sanchez, M. Rincon and I. Mora-Sero, *J. Phys. Chem. Lett.*, 2015, **6**, 1883–1890.
110 N. Yantara, S. Bhaumik, F. Yan, D. Sabba, H. A. Dewi, N. Mathews, P. P. Boix, H. V. Demir and S. Mhaisalkar, *J. Phys. Chem. Lett.*, 2015, **6**, 4360–4364.
111 A. Genco, F. Mariano, S. Carallo, V. L. P. Guerra, S. Gambino, D. Simeone, A. Listorti, S. Colella, G. Gigli and M. Mazzeo, *Adv. Electron. Mater.*, 2016, **2**, 1500325.
112 N. Wang, L. Cheng, J. Si, X. Liang, Y. Jin, J. Wang and W. Huang, *Appl. Phys. Lett.*, 2016, **108**, 141102.
113 Z. F. Shi, X. G. Sun, D. Wu, T. T. Xu, S. W. Zhuang, Y. T. Tian, X. J. Li and G. T. Du, *Nanoscale*, 2016, **8**, 10035–10042.
114 Y. H. Kim, H. Cho, J. H. Heo, S. H. Im and T. W. Lee, *Curr. Appl. Phys.*, 2016, **16**, 1069–1074.
115 D. Bin Kim, J. C. Yu, Y. S. Nam, D. W. Kim, E. D. Jung, S. Y. Lee, S. Lee, J. H. Park, A. Y. Lee, B. R. Lee, D. Di Nuzzo, R. H. Friend and M. H. Song, *J. Mater. Chem. C*, 2016, **4**, 8161–8165.
116 X. F. Zhao, B. H. Zhang, R. Y. Zhao, B. Yao, X. J. Liu, J. Liu and Z. Y. Xie, *J. Phys. Chem. Lett.*, 2016, **7**, 4259–4266.
117 Z. B. Wang, T. Cheng, F. Z. Wang, S. Y. Dai and Z. A. Tan, *Small*, 2016, **12**, 4412–4420.
118 Z. H. Wei, A. Perumal, R. Su, S. Sushant, J. Xing, Q. Zhang, S. T. Tan, H. V. Demir and Q. H. Xiong, *Nanoscale*, 2016, **8**, 18021–18026.
119 Z. Shi, Y. Li, Y. Zhang, Y. Chen, X. Li, D. Wu, T. Xu, C. Shan and G. Du, *Nano Lett.*, 2017, **17**, 313–321.
120 J. Li, L. Xu, T. Wang, J. Song, J. Chen, J. Xue, Y. Dong, B. Cai, Q. Shan, B. Han and H. Zeng, *Adv. Mater.*, 2017, **29**, 1603885.
121 J. Song, J. Li, X. Li, L. Xu, Y. Dong and H. Zeng, *Adv. Mater.*, 2015, **27**, 7162–7167.
122 N. Wang, L. Cheng, R. Ge, S. Zhang, Y. Miao, W. Zou, C. Yi, Y. Sun, Y. Cao, R. Yang, Y. Wei, Q. Guo, Y. Ke, M. Yu, Y. Jin, Y. Liu, Q. Ding, D. Di, L. Yang, G. Xing, H. Tian, C. Jin, F. Gao, R. H. Friend, J. Wang and W. Huang, *Nat. Photonics*, 2016, **10**, 699–704.
123 H. Hu, T. Salim, B. Chen and Y. M. Lam, *Sci. Rep.*, 2016, **6**, 33546.
124 M. Yuan, L. N. Quan, R. Comin, G. Walters, R. Sabatini, O. Voznyy, S. Hoogland, Y. Zhao, E. M. Beauregard, P. Kanjanaboos, Z. Lu, D. H. Kim and E. H. Sargent, *Nat. Nanotechnol.*, 2016, **11**, 872–877.
125 A. Sadhanala, S. Ahmad, B. D. Zhao, N. Giesbrecht, P. M. Pearce, F. Deschler, R. L. Z. Hoye, K. C. Godel, T. Bein, P. Docampo, S. E. Dutton, M. F. L. De Volder and R. H. Friend, *Nano Lett.*, 2015, **15**, 6095–6101.
126 J. Byun, H. Cho, C. Wolf, M. Jang, A. Sadhanala, R. H. Friend, H. Yang and T. W. Lee, *Adv. Mater.*, 2016, **28**, 7515–7520.

 

127 W. S. M. Wei, Y. Liu, Z. Liu, L. Xiao, Z. Bian and Z. Chen, *Phys. Status Solidi A*, 2016, **213**, 2727–2732.
128 D. Liang, Y. L. Peng, Y. P. Fu, M. J. Shearer, J. J. Zhang, J. Y. Zhai, Y. Zhang, R. J. Hamers, T. L. Andrew and S. Jin, *ACS Nano*, 2016, **10**, 6897–6904.
129 G. R. Li, Z. K. Tan, D. W. Di, M. L. Lai, L. Jiang, J. H. W. Lim, R. H. Friend and N. C. Greenham, *Nano Lett.*, 2015, **15**, 2640–2644.
130 Y. C. Ling, Z. Yuan, Y. Tian, X. Wang, J. C. Wang, Y. Xin, K. Hanson, B. W. Ma and H. W. Gao, *Adv. Mater.*, 2016, **28**, 305–311.
131 A. Kojima, K. Teshima, Y. Shirai and T. Miyasaka, *J. Am. Chem. Soc.*, 2009, **131**, 6050–6051.
132 J. H. Im, C. R. Lee, J. W. Lee, S. W. Park and N. G. Park, *Nanoscale*, 2011, **3**, 4088–4093.
133 *Nat. Mater.*, 2014, **13**, 837.
134 X. Y. Zhu, *Acc. Chem. Res.*, 2016, **49**, 355–356.
135 H.-S. Kim, C.-R. Lee, J.-H. Im, K.-B. Lee, T. Moehl, A. Marchioro, S.-J. Moon, R. Humphry-Baker, J.-H. Yum, J. E. Moser, M. Grätzel and N. G. Park, *Sci. Rep.*, 2012, **2**, 591.
136 M. M. Lee, J. Teuscher, T. Miyasaka, T. N. Murakami and H. J. Snaith, *Science*, 2012, **338**, 643–647.
137 J. Burschka, N. Pellet, S.-J. Moon, R. Humphry-Baker, P. Gao, M. K. Nazeeruddin and M. Gratzel, *Nature*, 2013, **499**, 316–319.
138 M. Liu, M. B. Johnston and H. J. Snaith, *Nature*, 2013, **501**, 395–398.
139 H. P. Zhou, Q. Chen, G. Li, S. Luo, T. B. Song, H. S. Duan, Z. R. Hong, J. B. You, Y. S. Liu and Y. Yang, *Science*, 2014, **345**, 542–546.
140 W. S. Yang, J. H. Noh, N. J. Jeon, Y. C. Kim, S. Ryu, J. Seo and S. I. Seok, *Science*, 2015, **348**, 1234–1237.
141 M. Saliba, T. Matsui, J. Y. Seo, K. Domanski, J. P. Correa-Baena, M. K. Nazeeruddin, S. M. Zakeeruddin, W. Tress, A. Abate, A. Hagfeldt and M. Gratzel, *Energy Environ. Sci.*, 2016, **9**, 1989–1997.
142 National Renewable Energy Laboratory (NREL) Best Research Cell. Efficiency chart. http://www.nrel.gov/ncpv/images/efficiency_chart.jpg, 2016.
143 J. You, L. Meng, T.-B. Song, T.-F. Guo, Y. Yang, W.-H. Chang, Z. Hong, H. Chen, H. Zhou, Q. Chen, Y. Liu, N. De Marco and Y. Yang, *Nat. Nanotechnol.*, 2016, **11**, 75–81.
144 F. Li, C. Ma, H. Wang, W. Hu, W. Yu, A. D. Sheikh and T. Wu, *Nat. Commun.*, 2015, **6**, 8238.
145 M. Kaltenbrunner, G. Adam, E. D. Glowacki, M. Drack, R. Schwodiauer, L. Leonat, D. H. Apaydin, H. Groiss, M. C. Scharber, M. S. White, N. S. Sariciftci and S. Bauer, *Nat. Mater.*, 2015, **14**, 1032–1039.
146 J. H. Noh, S. H. Im, J. H. Heo, T. N. Mandal and S. I. Seok, *Nano Lett.*, 2013, **13**, 1764–1769.
147 C. R. Kagan, D. B. Mitzi and C. D. Dimitrakopoulos, *Science*, 1999, **286**, 945–947.
148 M. Safdari, P. H. Svensson, M. T. Hoang, I. Oh, L. Kloo and J. M. Gardner, *J. Mater. Chem. A*, 2016, **4**, 15638–15646.
149 D. B. Mitzi, S. Wang, C. A. Feild, C. A. Chess and A. M. Guloy, *Science*, 1995, **267**, 1473–1476.
150 B.-E. Cohen, M. Wierzbowska and L. Etgar, *Adv. Funct. Mater.*, 2016, DOI: 10.1002/adfm.201604733.
151 L. N. Quan, M. J. Yuan, R. Comin, O. Voznyy, E. M. Beauregard, S. Hoogland, A. Buin, A. R. Kirmani, K. Zhao, A. Amassian, D. H. Kim and E. H. Sargent, *J. Am. Chem. Soc.*, 2016, **138**, 2649–2655.
152 G. Grancini, C. Roldán-Carmona, I. Zimmermann, D. Martineau, S. Narbey, F. Oswald and M. K. Nazeeruddin, 2016, arXiv preprint arXiv:1609.09846.
153 D. Kufer and G. Konstantatos, *ACS Photonics*, 2016, **3**, 2197–2210.
154 I. Dursun, C. Shen, M. R. Parida, J. Pan, S. P. Sarmah, D. Priante, N. Alyami, J. Liu, M. I. Saidaminov, M. S. Alias, A. L. Abdelhady, T. K. Ng, O. F. Mohammed, B. S. Ooi and O. M. Bakr, *ACS Photonics*, 2016, **3**, 1150–1156.
155 I. Suarez, E. J. Juarez-Perez, J. Bisquert, I. Mora-Sero and J. P. Martinez-Pastor, *Adv. Mater.*, 2015, **27**, 6157–6162.
156 Z. Y. Wang, J. Y. Liu, Z. Q. Xu, Y. Z. Xue, L. C. Jiang, J. C. Song, F. Z. Huang, Y. S. Wang, Y. L. Zhong, Y. P. Zhang, Y. B. Cheng and Q. L. Bao, *Nanoscale*, 2016, **8**, 6258–6264.
157 Q. Lin, A. Armin, P. L. Burn and P. Meredith, *Nat. Photonics*, 2015, **9**, 687–694.
158 S. Yakunin, M. Sytnyk, D. Kriegner, S. Shrestha, M. Richter, G. J. Matt, H. Azimi, C. J. Brabec, J. Stangl, M. V. Kovalenko and W. Heiss, *Nat. Photonics*, 2015, **9**, 444–449.
159 H. Wei, Y. Fang, P. Mulligan, W. Chuirazzi, H.-H. Fang, C. Wang, B. R. Ecker, Y. Gao, M. A. Loi, L. Cao and J. Huang, *Nat. Photonics*, 2016, **10**, 333–339.
160 Y. Guo, C. Liu, H. Tanaka and E. Nakamura, *J. Phys. Chem. Lett.*, 2015, **6**, 535–539.
161 S. Yakunin, D. N. Dirin, Y. Shynkarenko, V. Morad, I. Cherniukh, O. Nazarenko, D. Kreil, T. Nauser and M. V. Kovalenko, *Nat. Photonics*, 2016, **10**, 585–589.
162 J. Song, L. Xu, J. Li, J. Xue, Y. Dong, X. Li and H. Zheng, *Adv. Mater.*, 2016, **28**, 4861–4869.
163 J. C. Zhou, Y. L. Chu and J. Huang, *ACS Appl. Mater. Interfaces*, 2016, **8**, 25660–25666.
164 G. Maculan, A. D. Sheikh, A. L. Abdelhady, M. I. Saidaminov, M. A. Haque, M. Banavoth, E. Alarousu, O. F. Mohammed, T. Wu and O. M. Bakr, *J. Phys. Chem. Lett.*, 2015, **6**, 3781–3786.
165 S. Ahmad, P. K. Kanaujia, H. J. Beeson, A. Abate, F. Deschler, D. Credgington, U. Steiner, G. V. Prakash and J. J. Baumberg, *ACS Appl. Mater. Interfaces*, 2015, **7**, 25227–25236.
166 L. Lv, Y. Xu, H. Fang, W. Luo, F. Xu, L. Liu, B. Wang, X. Zhang, D. Yang, W. Hu and A. Dong, *Nanoscale*, 2016, **8**, 13589–13596.